Hybrid interface engineering in ZnPc/C_{60} bi-layer heterojunction organic solar cells

vorgelegt von
Diplom-Chemiker
Ivelin Bochukov
Weliko Tarnowo, Bulgarien

Von der Fakultät II – Mathematik und Naturwissenschaften
der Technischen Universität Berlin
zur Erlangung des akademischen Grades
Doktor der Naturwissenschaften
Dr.rer.nat.

genehmigte Dissertation

Promotionsausschuss:
Vorsitzender: Prof. Dr. Michael Gradzielski
Berichter/Gutachter: Prof. Dr. Arne Thomas
Berichter/Gutachter: Dr. Konstantinos Fostiropoulos

Tag der wissenschaftlichen Aussprache: 26 November 2012

Berlin 2013

D 83

Prepared at Helmholtz-Zentrum-Berlin, Berlin, department “Heterogeneous Materials Systems”, in the group “Organic Solar Cells” of Dr. Konstantinos Fostiropoulos

1st reviewer: Prof. Dr. Arne Thomas
2 nd reviewer: Dr. Konstantinos Fostiropoulos

I would like to dedicate this dissertation to my father Nikola Bochukov, who passed away on August 10th, 2011, when I was writing this work.

List of Abbreviations

OSC: Organic solar cells

ZnPc: Zn-phthalocyanine

BCP: Bathocuproine; 2,9-Dimethyl-4,7-diphenyl-1,10-phenanthroline

ITO: Indium-tin Oxide

TCO: Transparent conductive oxide

η: Power conversion efficiency

J_{sc}: Short circuit current dencity [A/cm^2]

Voc: Open circuit voltage [V]

P_{light}: Power of light reaching a solar cell

P_{max}: Maximal electrical power of a solar cell

R_p: Parallel resistance in a solar cell

R_s: Serial resistance in a solar cell

QCDC: Quartz crystal deposition controllers

PEDOT: PSS: Poly-ethylene dioxythiophene : poly-styrene sulphonate

UV-Vis: Ultraviolet-visible spectroscopy

XPS: X- ray photoelectron spectroscopy

XRD: X- ray diffraction spectroscopy

NEXAFS: Near edge x-ray absorption fine structure spectroscopy

SEM: Scanning electron microscopy

FTIR: Furier transform infrared spectroscopy

TABLE OF CONTENTS

1 Introduction and motivation

As the world is becoming advanced in technology the amount of big companies which produce electronic devices is growing fast, giving to every human the opportunity to use many of them every single day. This fact leads to more and more energy consumption. The demand of energy is strongly growing up over the past years [1]. The fossil fuels that are widely used today are running low, and also are harmful for the environment [2]. The earth is warming up and climates are changing. Fortunately, our beautiful planet gives us sunlight, flowing water and strong winds, which could be converted into energy. All these energy sources are abundant and free to use. We only must be sure that we convert the energy the right way, without causing other problems that can again hurt our environment.

Hardly the French scientist Edmond Bequerel, who in 1839 observed electric potential between two electrodes attached to a solid system upon light irradiation, knew that his just founded photovoltaic effect would have such a big meaning to our planet today [3]. This simple concept for conversion of sun power into electricity is in the basics of solar cells, which are a hot topic for research and development. This statement relays on the fact that with solar cells, power can be produced near the end user of the electricity, thus avoiding transmission losses and costs. The solar panels themselves operate without noise, toxic and greenhouse gas emissions, and require very little maintenance. Furthermore, the huge theoretical potential and the very high practical potential of the solar electricity make it attractive for large-scale utilization [4].

1.1 Organic photovoltaic cells

Over recent years, the photovoltaic market is formed almost only by sales of inorganic devices, which are based on silicon wafers. Silicon wafers are expensive and raise the cost of the final product [5]. Cheaper alternatives to the inorganic solar cells are the organic ones. The first generation of organic solar cells (OSCs) is based on single layers of organic molecules sandwiched between two metal electrodes with different work functions [6]. The reposted power conversion efficiencies η for this cell architecture in the beginning are only in the range of 10^{-3} to 10^{-2} %. But, in 1978 merocyanine dyes are placed between metal-metal oxide and a metal electrode and η of the solar cell reaches remarkable 0.7 % [7].

In 1986 Dr. Ching Tang at Kodak research laboratories was placing two organic dyes (a phthalocyanine derivative and a perylene derivative) between tin-doped InO_3 and gold electrodes. He creates the first organic solar cell with donor and acceptor material, and report 1% η [8]. This result determines OSCs as promising cheap alternative to the inorganic ones and cause many scientists all over the world to work on their improvement. The motivation for development of OSC is not only the lower price compared to the inorganic ones, but also simplicity in the production techniques, and the opportunity to be prepared on plastic foils, which makes them suitable for flexible and portable systems [9].

The potential of semiconducting organic materials to transport electric current and to absorb light in the ultraviolet, visible and infrared part of the solar spectrum is due to sp^2 hybridization of carbon atoms in a long conjugated π-system [10]. For example in a molecule like phthalocyanine the electron on the p_z- orbital of each sp^2 hybridized carbon atom is forming π- bonding with the other p_z- electrons from the neighboring carbons which leads to conjugated π-system. Due to isomeric effect these π electrons are delocalized resulting in high electronic polarizability.

Depending on the materials that are used for their preparation, three different

types of organic solar cells are known. Solar cells prepared with small molecules, polymer solar cells and the so called dye-sensitised (or Grätzel) cells which contain dye molecules adsorbed on electron transporting layer of highly porous titanium dioxide.

1.2 Bilayer heterojunction solar cell architecture

In this work we are dealing with a bilayer heterojunction solar cell architecture based on small molecules (**Figure 1**). Two absorbers, Zn-phthalocyanine (ZnPc) as p-type (hole transporting) material and fullerene-C_{60} as n-type (electron transporting) material are sandwiched between front indium-tin oxide (ITO) and back aluminum (Al) electrodes. Beside the active layers and the back electrode there is also a buffer layer Bathocuproine (BCP), (2,9-dimethyl-4,7-diphenyl-1,10-phenanthroline) whose role is to admit only electrons to pass to the Al electrode.

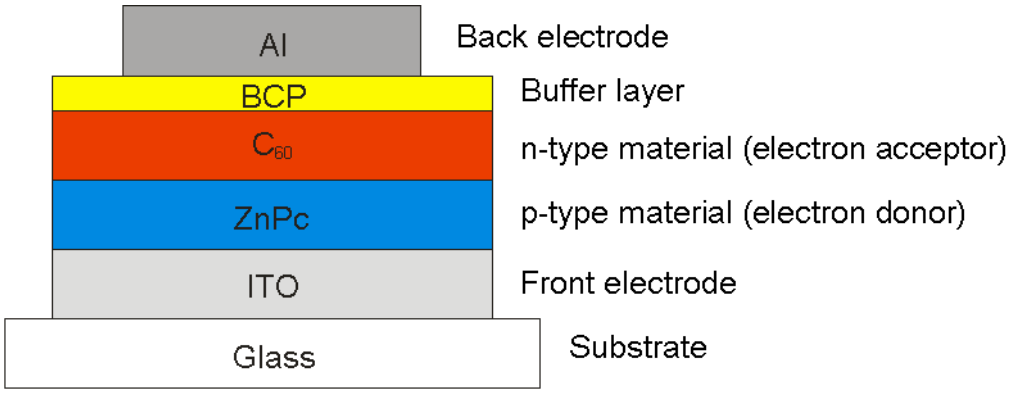

Figure 1. Bilayer heterojunction solar cells architecture based on Zn-phthalocyanine as electron donor and C_{60} as an electron acceptor. The two materials are sandwiched between ITO (front) and Al (back) electrodes. Under the back electrode, electron transparent buffer layer, Bathocuproine (BCP) is placed.

The thickness of the organic semiconductors in the device is limited by the low charge carrier mobility and exciton diffusion length, whose value lies between 10 and 100 nm. However organic semiconductors have strong absorption coefficients usually in the range of $\geq 10^5$ cm^{-1} giving them high absorption even in layers with thickness less than 100 nm [11].

After optimization procedure, an optimal layer thickness for each material in our device was found. High efficiency was achieved by a solar cell with the following configuration: ZnPc 30 nm, C_{60} 30 nm, BCP 10 nm, Al 100 nm.

1.3 Energy diagram and functioning principal of the solar cell

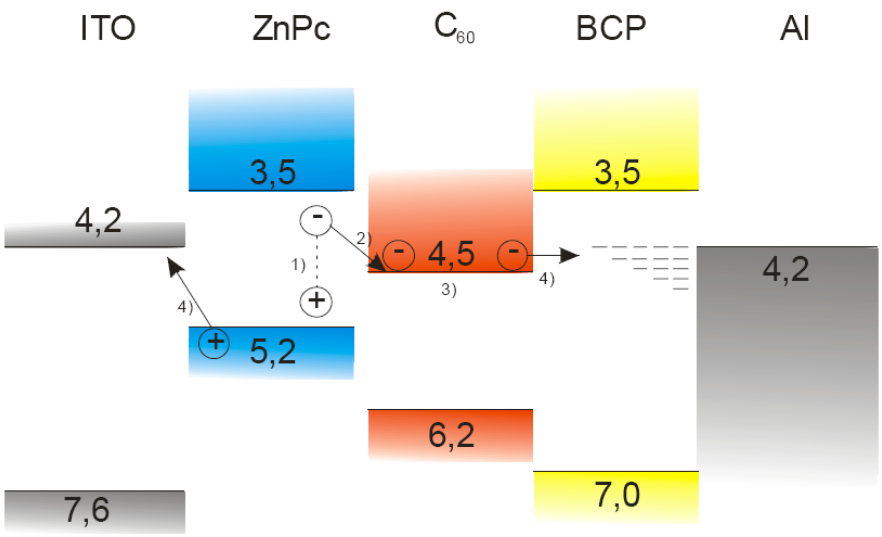

Figure 2. Energy level diagram of bilayer heterojunction solar cell. Values are given in eV. Process 1) Absorption of light and creation of charges; process 2) Exciton diffusion; process 3) Exciton separation at D/A interface; process 4) Charge transport to electrodes; process 5) Collection of charges

The fundamental difference between the working principles of inorganic and organic solar cells is in the direct generation of free charge carriers in the inorganic solar cells. In OSC the absorption of sun light is followed by generation of excitons which are pairs of electrons and holes held together due to coulomb interactions with a typical binding energy of 0.3- 0.5 eV [12]. To generate a photocurrent the excitons must be dissociated into free electrons and holes. The excitons first move via diffusion to the interface between the electron donor and acceptor material. There the difference in the electronic levels of the two materials provides the necessary energetic driving force for their dissociation [13]. After excitons are dissociated they have to be transported to the electrodes. Energy level diagram for the solar cells which is an object of discussion in this work is sketched on **Figure 2**. In our device, electrons are transported through the C_{60}'s lowest unoccupied molecular orbital (LUMO) and holes through the ZnPc highest occupied molecular orbital (HOMO). The last step is charge extraction at the electrodes. Electrons go through the BCP buffer

and are collected at the Al cathode. Holes are collected at the ITO anode.

In general, for a successful organic photovoltaic cell the five important processes have to be optimized to obtain a high power conversion efficiency of solar energy into electrical energy:

- Light absorption
- Exciton transport
- Charge carrier generation
- Charge carrier transport
- Charge collection

1.4 TCO morphology and hybrid interface engineering

In this work we are dealing with the problems at the hybrid interface between the TCO anode and the first organic layer. TCO films are usually prepared by sputtering process on glass substrates. Such prepared films have highly active surfaces where the unsaturated open bindings form charge carrier traps. In other words the TCO surface is positively charged which on one hand limits the charge carrier extraction at the hybrid interface. On the other hand it leads to exciton and charge recombination in the bulk and also to space charge limited donor/acceptor interface. Furthermore, in bi-layer solar cell architectures an interface energetic barrier between the Fermi level of the inorganic anode (in our case ITO) and the HOMO level of the organic semiconductor is present, which prevents fast charge transport and extraction through this interface [15]. Common solution for all these interface problems is an additional buffer layer to be introduced at the hybrid interface. Usually this is the block co-polymer, polyethylenedioxythiophene:polystyrenesulphonate (PEDOT:PSS), **Figure 3** [13,16,17].

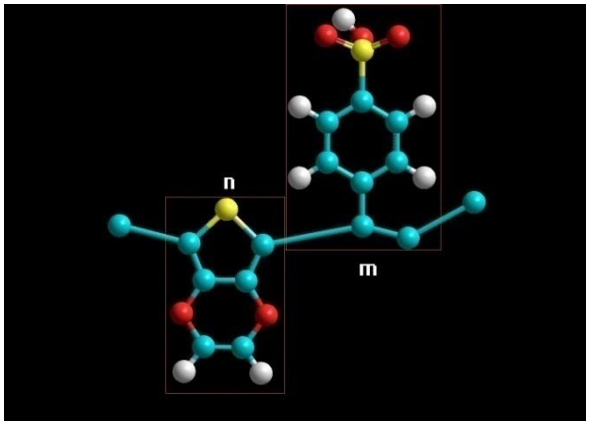

Figure 3. Structural formula of polyethylenedioxythiophene:polystyrenesulphonate (PEDOT:PSS), commonly used as front buffer layer in organic solar cells.

However PEDOT:PSS possess a number of drawbacks. It has an optical absorption in the visible range, which diminishes the absorption of sun light in

the active layers of the device. Additionally it was observed that introducing this buffer layer results in degradation problems due to its water absorption, even after annealing [18]. Furthermore the PSS part of this copolymer is easy to diffuse into other parts of the device and possibly react with other components [19]. As a result, decrease of short-circuit current (I_{sc}) fill factor (FF) and power conversion efficiency η is observed [20]. Last but not least PEDOT:PSS is being deposited by the industrially non-relevant spin-coating process [21]. One approach in this work is to develop PEDOT:PSS free OSC. We propose to synthesize functional phthalocyanine derivatives and to apply them wet-chemically on the ITO surface. The new molecules would passivate surface traps and modify the ITO work function so that the energetic barrier is reduced.

Another approach is to give morphology to the ITO substrate. A rough substrate surface would scatter the incoming sun light and thus increase the absorption in the absorber materials. Furthermore the TCO morphology is desirable to increase the active surface area at the D/A interface leading to more efficient generation of free charge carriers [22].

Molecular orientation of the absorbers can significantly affect their material characteristics such as light absorption, charge transport and energy level in the film which are detrimental for efficient device performance [23,24]. For planar π-conjugated molecules the charge transport is favored along the stacking axis due to the strong π-coupling between neighboring molecules, while the transport perpendicular to the stacking axis is less efficient [25,26,27]. In organic solar cells where the desired charge transport direction is perpendicular to the substrates surface, a vertical π-π stacking of aromatic molecules is highly desirable. In literature some studies on alignment of the molecular stacking of organic films to the charge transport direction can be found. MO_3, WO_3, NiO, V_2O_5 have been used as buffer layer on ITO in order to change the molecular orientation of the absorber molecules and to facilitate hole collection from the ITO anode [28,29,30].

For the molecular reorientation of our absorber material we decided to use copper I iodide (CuI) as template. CuI is a solid with three crystalline phases α, β and γ. The high temperature (above 392 °C), α -phase has a cubic structure. The β hexagonal phase is an ionic conductor. The low-temperature (below 350 °C) γ -phase again of cubic structure is a p-type semiconductor with a band gap of 3.1 eV, whose conductivity depends on the presence of iodine in stoichiometric excess [31]. The crystal structure of γ -CuI which is an object of discussion in this thesis can be seen on **Figure 4**.

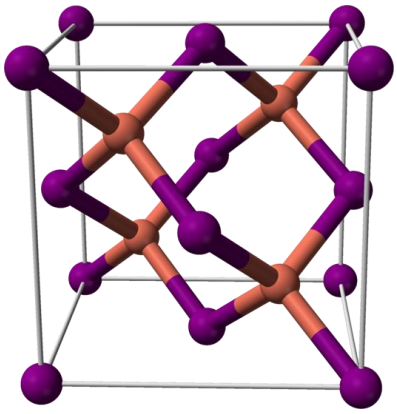

Figure 4. Crystalline structure of γ -copper I iodide (CuI).

Also CuI has high transparency in the visible and near infrared regions and can be deposited by vacuum thermal evaporation. Additionally is a dipole molecule which suggests high work function. Deposited as thin layer at the front electrode of the solar cell, CuI could reduce the energetic barrier to the hole collection. An iodide ion (I^{-1}) is one of the largest monoatomic anions. It has a radius of 220 picometers. Iodide ion is high reactive and when the absorber molecules (in our case ZnPcs) are deposited on top of CuI substrate, strong substrate-molecule interactions are expected. When the substrate-molecule interaction is stronger than the molecule-molecule interaction, the molecules change their orientation and lay parallel to the substrate.

Knowing all problems of the bilayer heterojunction solar cell and having in mind the possible solution for them, we can define the topics and goals of the present work.

1.5 Topics and goals of the present work

- Chemically engineer the hybrid interface in bilayer OSC with functionalized organic molecules in order to passivate surface traps and reduce energetic barrier.
- Introduce ZnO, mesoporous ITO and ITO fibers as TCO anode with high morphology in OSC.
- Study the substrate morphology effects on the light absorption and charge transport at the TCO-organic interface.
- Create an interface for oriented growth of the absorber molecules in order to improve the charge carrier transport and absorption of light in the device.

2 Experimental part: Reagents, Syntheses, Methods

Since the production of material for photovoltaic and photovoltaic devices requires high purity, the experiments done in this thesis were performed with serious consideration of chemical purity and clean environments.

2.1 Environments

Substrate washing, spin-coating and ITO termination dipping procedures were performed in a Laminar-flow Box from Micro CleanRoom Technology GmbH with an "Astrocell II®" air cleaning facility.

Applications which needed protection from humidity or air oxygen have been performed in an InterTec GmbH Glove Box, under nitrogen gas with impurities less than 1 ppm.

Evaporation of organic materials for the production of solar cells has been done in a Balzers ultra-high-vacuum (UHV) evaporation chamber under pressure of about 10^{-8} mbar.

Chemical synthetic preparations, sensitive to humidity have been performed in a fume hood, with glassware.

2.2 Chemicals, reagents and materials

ZnPc used for the device preparation through UHV evaporation is delivered from "Alfa Aesar" with 90 % purity. Because of the low purity grade the material was additionally purified twice through vacuum sublimation. Sublimation purified C_{60} was delivered from "MER" with purity 99.9 %. BCP was obtained from "Fluka" with purity $\geq$ 97 % and used in the production process without further purification. Al for the back contact of the solar cell was obtained from "Alfa Aesar" with purity 99.9 %

Precursors for the syntheses of TCO termination molecules were delivered from Sigma Aldrich.

ITO (310 nm) sputtered on polished float glass substrates with square resistance

5 Ω and 7 Ω were delivered by Präzisions Glas & Optic GmbH, readily cut in 24/13 mm size.

Mesoporous ITO (100 nm) prepared by sol-gel process on the described above commercial ITO substrates were provided by the group of Professor Bernd Smarsly, Physikalisch-Chemisches Institut, Justus Liebig Universität Gießen.

2.3 Synthesis of molecules

TCOs surface has to be modified in order to adjust its properties to the requirements of the organics.

Such an adjustment can be done with a phthalocyanine molecule consisting three or four valent central metal atom where organic polar ligand could be attached. The polar ligand increases the surface work function and passivates open bindings, whereas the aromatic macrocycle system forms a π-π interface with the adjacent organic absorber (**Figure 5**). For this purpose we decided to synthesize a novel axially substituted phthalocyanine, attaching gallic acid to the Sn (IV)-phthalocyanine.

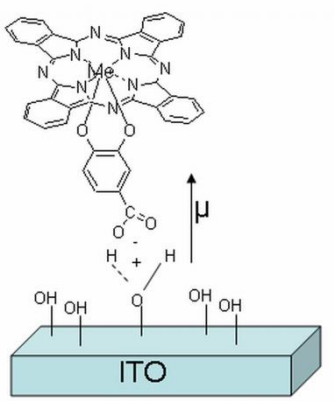

Figure 5. Sputter grown ITO is terminated by polar aromatic molecule, applying dip-coating techniques. The polar ligand increases the surface work function and passivates open bondings, whereas the aromatic macrocycle system forms a π-π interface with the adjacent organic absorber.

These molecules allow TCO termination by dip-coating technique which is industrially relevant.

2.3.1 Sn-phthalocyanine with an axial gallic acid rest

Axially modified Sn-phthalocyanine with gallic acid rest was obtained in one step ligand exchange reaction through the following procedure:

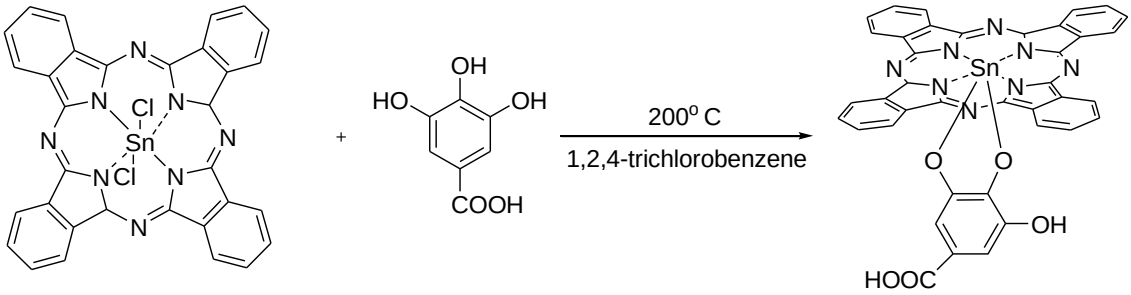

0.5 g of Ti (IV)- phthalocyanine dichloride were dispersed in 20 ml 1,2,4-trichlorobenzene, and 0.6 g gallic acid were added. The suspension is heated up to 200° C for two hours. After cooling to room temperature the reaction mixture was filtered and washed with benzene, hexane and methanol. The reaction product was dried in vacuum at 60° C (Yield 33 %).

FTIR (KBr) ν = 580 s, 735 m, 753 m, 780 m, 880 m, 1089 s, 1120 s, 1300 vs, 1337 s, 1425 m, 1470 m, 1515 s, 1568 m, 1620 s, 1685 vs, 1700 s, 2585 s, 2800 s, 3100 s 3150 s, cm^{-1}.

2.3.2 Synthesis of 1,2-dibromo-4,5-bis(octyloxy)benzene

Well known fact is that, phthalocyanines have low solubility in organic solvents. The axially attached functional group increases its solubility but, those molecules are still not good soluble in organic solvents. In order to increase its solubility we decided to attach peripherally to the phthalocyanine macrocycle octyloxy groups. The alkyl groups also could act as template for epitaxial growth of the absorber molecules. The synthesis was carried out in four reaction steps, starting from dibromocatechol precursor. The procedure was adapted from that used by J.F. van der Pol *et al*. [32]

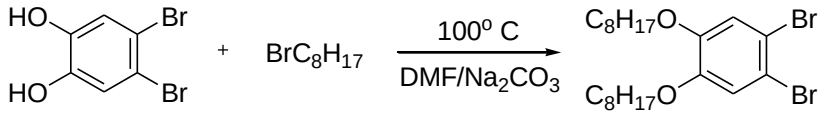

Dibromocatechol 3g (0.0112 mol) was dissolved in 20 ml DMF and 2,3 g Na_2CO_3 (0.0216 mol) was added to a solution. After 0.5 hours stirring 4,3 g of 1-bromooctane dissolved in 10 ml DMF was added dropwise. The dark borwn solution was heated to 100 °C and stirred for 12 hours. The reaction solution was poured into 55 ml 0.2 M HCl and the resulting product was extracted with 20 ml ether three times. The solvent was removed at rotary evaporator with yield about 12 ml brown oil.

2.3.3 Synthesis of 1,2-Dicyano-4,5-bis(octyloxy)benzene

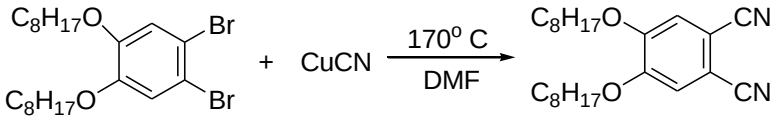

A solution of 11 ml 1,2-dibromo-4,5-bis(octyloxy)benzene and 6 g CuCN in 150 ml DMF were refluxed for 8 hours under dry nitrogen . The reaction was cooled to room temperature, than poured into 350 ml NH_4OH and stirred for 24 hours. The precipitate was filtrated and washed with water until the washings were neutral. The crude product was extracted in a Soxhlet apparatus with ether for 3 days. The solvent was evaporated to dryness and the product was additional purified by recristallization from hexane.

2.3.4 2,3,9,10,16,17,23,24-Octakis(octyloxy)phthalocyanine-iron (III) chloride

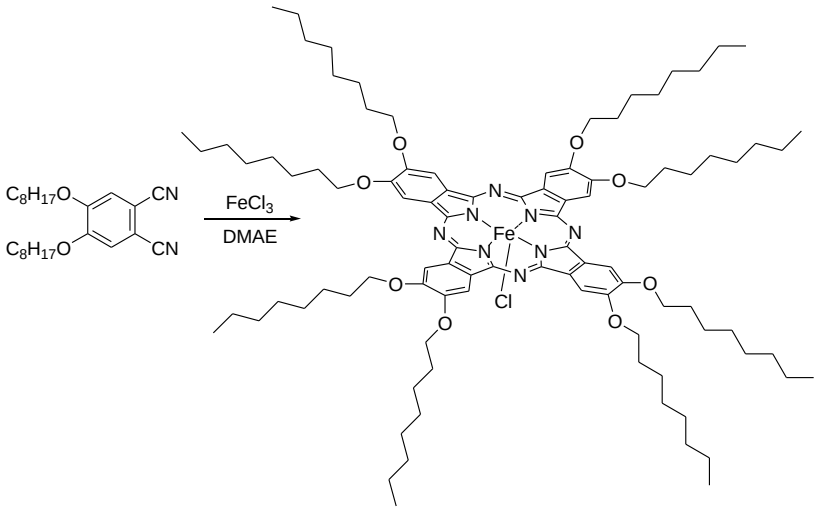

A mixture of 1g 1,2-Dicyano-4,5-bis(octyloxy)benzene and 71.8 mg anhydrous $FeCl_3$ were refluxed in 2-(dimethylamino)ethanol (DMAE) for 48 hour under a dry nitrogen atmospehere. The reaction mixture was cooled down to room temperature and diluted with 10 ml chloroform and than poured into 50 ml acetone. The precipitate was filtered and the residue was extracted with acetone, methanol and ether in a Soxhlet apparatus for 24 hours in each solvent. Yield 30%. FT-IR spectrum of the synthesized molecule is shown on **Figure 6**.

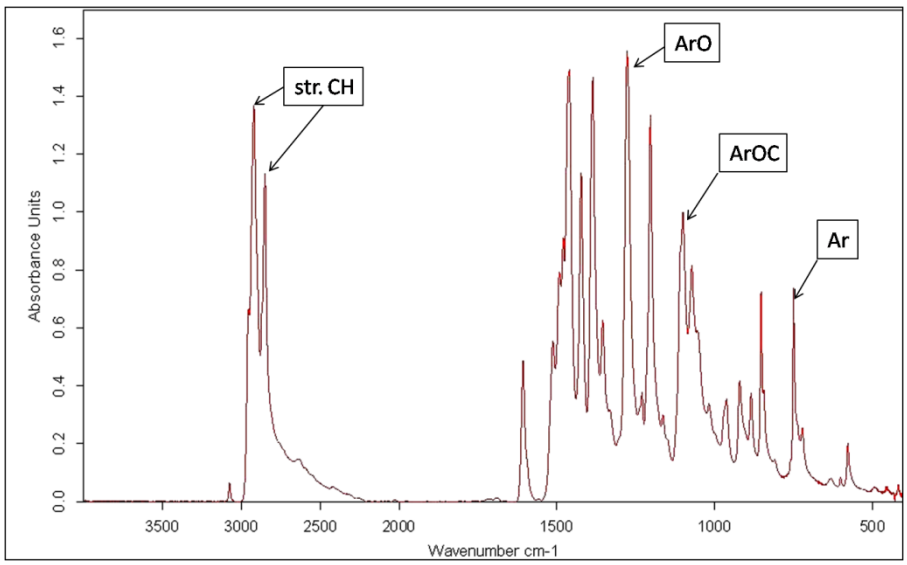

Figure 6. FT-IR spectrum of 2,3,9,10,16,17,23,24-Octakis(octyloxy)phtloacyanine-iron (III) chloride, measured in KBr matrix. 2840 cm^{-1} and 2905 cm^{-1} (str. CH), 1275 cm^{-1} (ArO), 1095 cm^{-1} (ArOC), 750 cm^{-1} (Ar).

2.3.5. Axial substitution of 2,3,9,10,16,17,23,24 octakis(octyloxy)phthalocyanine-iron (III) chloride

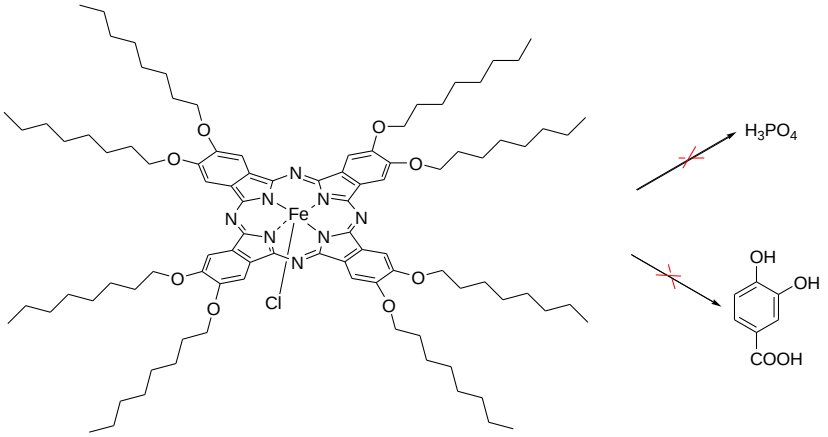

The long octyloxy groups sterically disturb the axial substitution. After experiments with two different ligands this reaction was determined as impossible. Nevertheless we decided to test 2,3,9,10,16,17,23,24-Octakis(octyloxy)phthalocyanine-iron (III) chloride as TCO termination material and to study its influence on the device performance.

2.4 Methods for film preparation

2.4.1 Electrochemical deposition of ZnO nanostructures

Electrochemistry could be described as the use of electricity to affect chemical processes or systems [33]. The mass transport in electrochemical cell can follow three mechanisms: migration, convection and diffusion [34]. Migration is the movement of ions under the influence of electric field. Convection is mass transport resulting from movement of the solution as a whole. Diffusion is mass transport driven by a gradient of chemical potential. When the concentration of a molecule or ions is uneven in the solution, mass transport will occur to restore its homogeneity.

In most electrochemical reactions the transport of electroactive species is affected by only one mechanism, which typically is diffusion.

A three-electrode electrochemical cell is most often used in electrochemical experiments and as well as is used in this work (**Figure 7**).

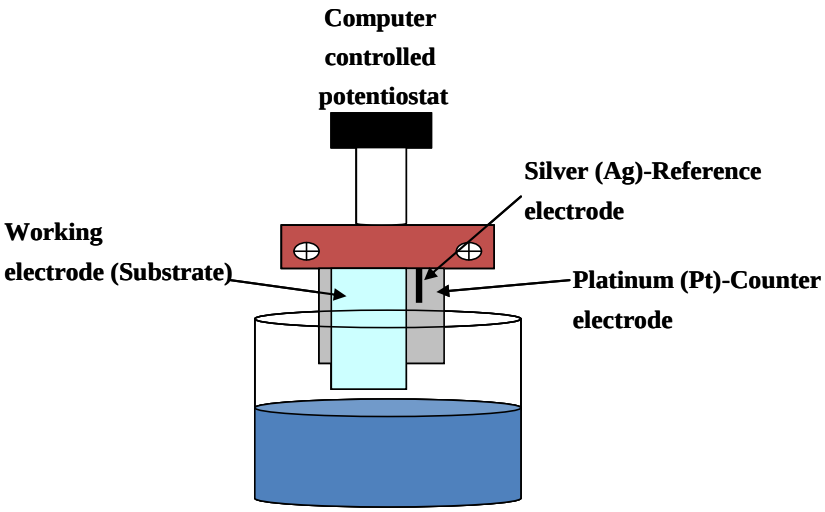

Figure 7. A conventional three-electrode electrochemical cell for deposition of ZnO nanostructures.

The electrochemical phenomena take place at the working electrode. In our case this is the ITO substrate on which we grow ZnO nanostructures. The geometry of this electrode must be considered for the electrochemical reaction [35].

The reference electrode is the electrode whose potential is constant enough and could be taken as standard against which the potential of the other electrodes in

the electrochemical cell can be measured. The ideal reference electrode is one whose potential does not shift from equilibrium [36]. For our cell we took silver (Ag) as reference electrode.

The counter electrode is the one who serves as a source for electrons, so that current can be passed from the external circuit thorough the cell. Platinum was chosen as counter electrode.

2.4.2 Cleaning procedure for TCO substrates

The presence of impurity in the cells interface can change the physical-chemistry properties of the organic molecules, and it will reflect onto the photovoltaic effect. That is why the solar cells production starts with thorough cleaning of TCO substrates. The cleaning procedure can be summarized as follows:

1. Mechanical wiping of ITO substrates with absolute ethanol for removing rough impurities as visible dust particles.
2. Ten minutes cleaning in a beaker with acetone in ultrasonic bath followed by rinsing of the substrates with 18 M (deionized water "MILLIPORE").
3. Ten minutes in ultrasonic bath in ethanol and rinsing with deionized water.
4. Ten minutes in a beaker with only deionized water for removing all organic solvents from the substrate's surface.
5. As a last step the substrates are dried with ionized nitrogen gas flow.

After the substrates were dried with nitrogen, water was still present on the TCO surface which was observed from the increased serial resistance in the solar cell. Annealing step for the substrates on a hot plate for 20 minutes at 120° C was carried out and the serial resistance in the device was improved. The annealing step was defined as standard for the preparation of all ITO substrates before production of solar cells.

2.4.3 TCO passivation

ITO substrates were terminated with axially and peripherally substituted phthalocyanines whose synthesis is described in **2.3.** the following way.
After cleaning ITO substrates were placed in a beaker. A saturated solution of the particular phthalocyanine derivative was added to cover the samples and the substrates were kept there for 20 minutes at room temperature. Thereafter the substrates were thoroughly rinsed with plenty of water, so that only the chemisorbed monolayer species remain on the ITO surface and all the physisorbed rest is removed.

2.4.4 Solar cell production by vacuum deposition

High Vacuum (HV) chamber was used for vapor-deposition of the organic layers in the solar cells. Its construction is shown in **Figure 8**.

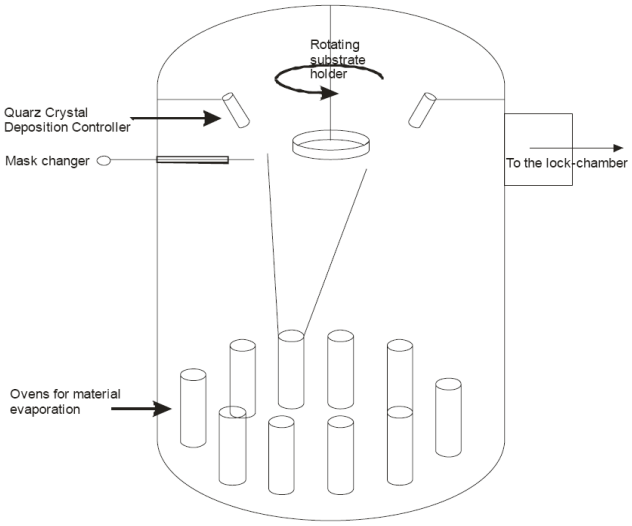

Figure 8. Schematic drawing of the HV evaporation chamber. Twelve ovens containing organic materials are situated at the bottom of the volume with the opening facing the substrate holder. Rotating substrate holder and quartz-crystal deposition controllers are near to each other in the upper part. A mask changer, perpendicular to the sample holder rotating axis, is situated at the level of the mask changing switch on the sample holder

This evaporation chamber is supplied with a pre-pump and turbo pump system and has a volume of around 300 liters. Twelve ovens containing organic substances are situated on the bottom of the chamber. The ovens are positioned

with their opening facing the substrate holder. **Figure 9** shows the construction of an oven.

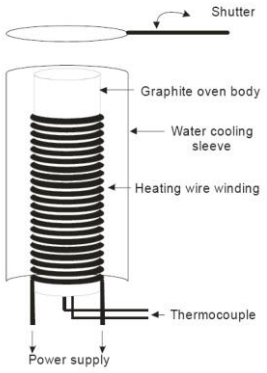

Figure 9. Schematic drawing of a graphite oven for material evaporation equipped with a tantalum heater, water cooling sleeve and metallic thermo-couple for temperature control

The structure of these ovens includes tantalum heater and a water cooling system which protects the surrounding from overheating. The shutter above the oven, with pneumatic control, must be opened before starting the evaporation. The temperature of the ovens is electronically controlled using metallic thermo-couple.

Layer deposition started with placing the sample holder in the lock chamber. Using a manipulator the holder was transported to a rotating head that turns continuously during the evaporation to guarantee homogenous growth of the deposited layers. Quartz-crystal deposition controllers are situated close to the rotating head for monitoring of the layer thickness and deposition rates. The deposition rate depends on the oven temperature. The organic layers in the solar cells were evaporated with an approximate deposition rate of 0.5 Å/sec (**Table 1**).

Layer	C_{60}	ZnPc	BCP	Aluminum
Oven temperature [°C]	500	400	120	1300

Table 1. Typical deposition temperatures at which the organic layers are evaporated with an approximate rate of 0.5 Å/sec

After deposition of the organic layers Al contacts were evaporated at 1300 degrees centigrade. A complete ZnPc/C_{60} bi-layer heterojunction organic solar cell is shown in **Figure 10**.

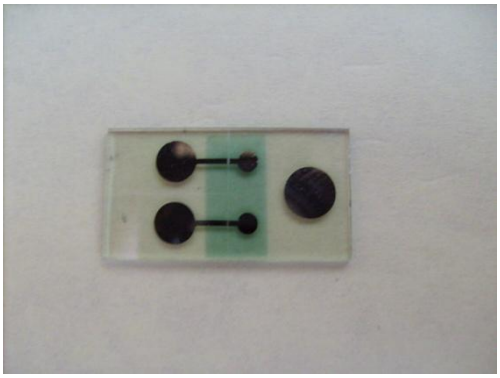

Figure 10. Photograph of two complete ZnPc/C_{60} bi-layer heterojunction organic solar cell, after organic layers and contacts deposition onto 1mm laser structured float-glass substrate with commercial 5 Ω/square ITO

After Al back contact evaporation, sample holder was transported through the lock chamber to a glove box using a manipulator. There under nitrogen atmosphere each cell was securely transferred to a specifically designed poly-acryl encapsulation (**Figure 11**).

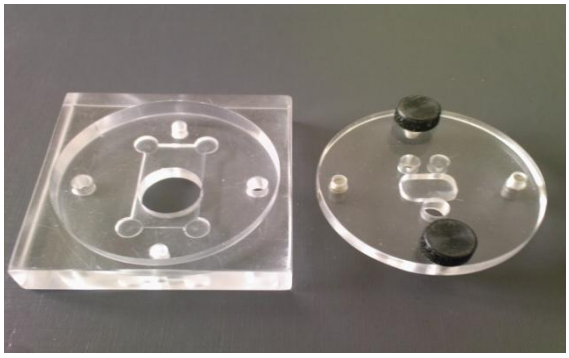

Figure 11. Solar cell encapsulation box (left) and lid (right).

In encapsulated state, degradation of the cells was inhibited. In this form all cells were taken out of the glove box and their I/V characteristics were measured under a sun simulator.

2.5 Analytical Methods

2.5.1 X-ray photoelectron spectroscopy (XPS)

In the present work, due to its surface sensitivity, XPS was chosen as a measurement technique for analyzing the surface work function of treated and untreated ITO substrates. ITO is a highly-doped n-type semiconductor. Its schematic energy diagram is shown in **Figure 12A**. The valence band and the conduction band are separated by the band gap (Eg), which for ITO is around 4 eV. In n-type semiconductors a Fermi level formed by the dopend is located within the band gap, very close to the conduction band. But, Fermi level has to be considered as theoretical construct since there are no allowed electronic states within the band gap. The Fermi level refers to the point on the energy scale where the probability to find an electron is 50 %. The work function (Φ) that we measure is the energy needed to excite an electron from the Fermi level to the vacuum level. XPS work function spectra are obtained when a material is irradiated with a monochromatic beam of x-rays and simultaneously kinetic energy and number of electrons that escape from the top 1 nm of the material is analyzed. This analytical technique is surface sensitive, because samples are irradiated only with soft x-rays produced by source with MgKα=1253.6 eV or AlKα=1486.6 eV spectrum. For our measurements Specs XR 50 x-ray tube with MgKα spectrum was used. The measurements were carried out with very low (10 W) x-ray power and additionally the source was placed at possible remote position from the sample (3.7 cm) in order to reduce the number of irradiated photons and thus receive information from only the very top layer of the analyzed material. Photoelectrons are ejected from the sample with a range of energies and directions. A series of focusing lenses collect one portion of these electrons, defined by those rays that can be transferred through the apertures and focused onto the analyzer entrance slit. Schematic drawing of the XPS instrument is shown in **Figure 12B**. The kinetic energy of emitted electrons was analyzed with hemispherical analyzer. Electrostatic fields within the energy

analyzer are established to only allow electrons of a given energy (the so called pass-energy) to arrive at the detector slits and onto the detector itself. The number of these electrons is counted by the detector. Detector pass-energy for all measurements was set to 3 eV, with accuracy ±0.1 eV. XPS must be carried out in ultra high vacuum due to the low energy of the photoenectrons which are easily absorbed in air or poor vacuum, but also to eliminate excessive surface contamination. Samples were analyzed at ultrahigh vacuum with pressure of 3×10^{-10} Mbar. With knowledge of the measured kinetic energy and the energy of the x-rays, energy conservation then allows us to determine the binding energy of the electron before it was ejected from the sample, using the equation:

$$E_{kin}=h\nu-E_B-\varphi$$

where E_{kin} is the kinetic energy of the ejected electron, hν is the photon energy, E_B is the binding energy of the electron in the solid, and φ is the work function of the detector. The peaks' positions in the measured spectra are proportional to the number of atoms of any kind from which the electrons are ejected, so that the stoichiometry of a sample can be identified, as well as the valence of chemical state of the internal elements.

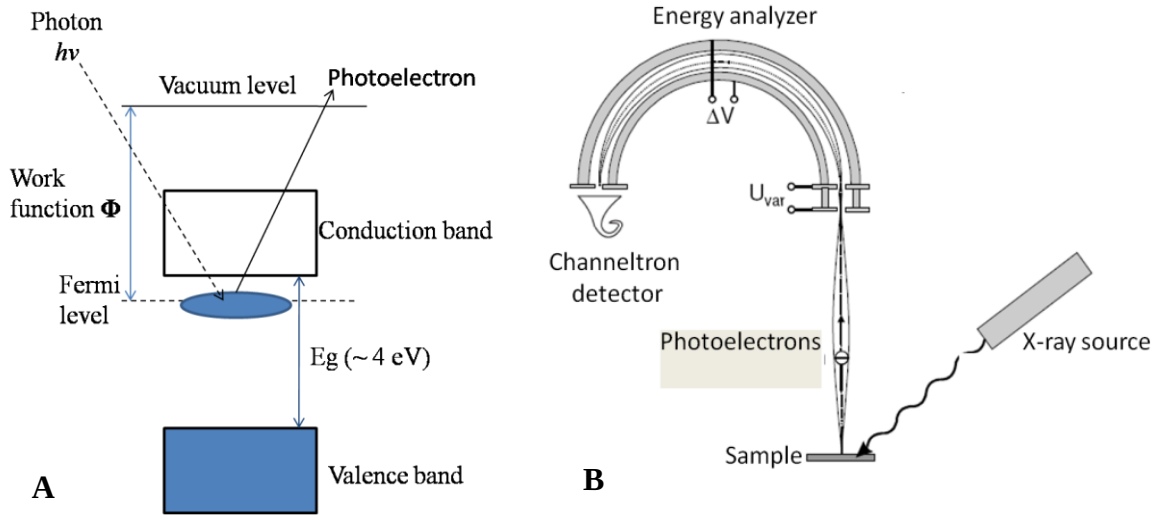

Figure 12. A(left), schematic energy diagram of ITO. B(right), x-ray photoelectron spectrometer with monochromatic x-ray source which irradiates the sample and produce electrons. The kinetic energy of the electrons is measured by energy analyzer and their number is counted by the electron detector.

2.5.2 Fourier transform infrared spectroscopy –FTIR

Molecular structures of the synthesized TCO termination molecules were verified through FTIR spectroscopy. In IR spectroscopy, when IR beam produced by IR source is passed through a sample, one part of the beam is absorbed by the sample and the rest is transmitted and transported to the detector. IR beam is absorbed, when the radiation frequency matches the vibrational frequency of a bond in the molecule. A molecule is infrared active only, when the vibrations of the bonds cause a change in the dipole moment of the molecule. Molecules with symmetric bonds as N_2 and O_2, do not absorb in the IR since bond stretching does not change the dipole moment.

IR spectra represent a fingerprint of a sample with absorption peaks which correspond to frequencies of vibrations between the bonds of the atoms making up the molecule. Therefore with IR spectroscopy qualitative analysis of every different kind of material can be carried out.

The preparation of our samples, measured in Potassium bromide (KBr) matrix includes grinding of solid product into KBr powder and pressing under vacuum in the form of a pellet. In our case all pellets weighed 300 mg. Before measuring the sample a background spectrum of the KBr matrix was recorded. Thus the characteristics of the matrix and the instrument were excluded from the sample's spectra. All samples were measured on a BRUKER FTIR spectrometer with resolution 2 cm^{-1}.

The original IR spectrometers are of the dispersive type. They separate the individual frequencies of energy emitted from the source. The detector measures the amount of energy at each frequency which has passed through the sample, which makes the scanning process slow. The main benefit of the FTIR spectrometers is that they make the scanning process much faster. A reason for that is the incorporated in these spectrometers interferometer between the IR source and the sample. The interferometer employs a beamsplitter which divides the incoming infrared beam into two optical beams. One beam is reflected by a

mirror with fixed position, while the other beam is reflected by a mirror which moves in a few millimeters distance. After the two beams are reflected by the respective mirror they recombine when meet back in the beamsplitter. The signal which exits the interferometer is a result of these two beams and is called interferogram. In the interferogram every data point which makes up the signal has information about every IR frequency which comes from the source. Ones the interferogram is measured, all frequencies are measured simultaneously, which makes the scanning process extremely fast. With help of the mathematical technique Fourier transformation, the measured interferogram can be converted into spectral information.

2.5.3 UV-Vis spectroscopy

Absorption of Zn-phthalocyanine deposited on different TCO substrates was determined with UV-Visible spectroscopy. All samples were measured on "Cary 500" UV-Vis spectrometer with integrating sphere (Ulbricht sphere) and 1 nm resolution. The integrating sphere is a useful tool for highly precise transmission and reflexion measurements on solid samples such as glass or plastics. These samples refract or distort the beam, causing it to hit different spots on the detector, which increases the amount of stray light in the system and the measured values are not reproducible. With the integrating sphere all reflected or transmitted light by the sample is captured in the sphere and focused in one spot of the detector, making the measured values reproducible.

Absorption spectra of the investigated samples were determined from UV-Vis data recorded in reflectance and transmission modes in the wavelength range between 250 and 800 nm. When sample molecules are exposed to light with enough energy for electronic transition within the molecule, some of the light energy is absorbed as the electron is promoted from bonding or non-bonding orbital to anti-bonding orbital. An absorption spectrum records the absorption of light as a function of wavelength.

The Beer-Lambert law, is the principle behind absorbance spectroscopy:

$$A = \log\left(\frac{I_0}{I}\right)$$

where A is the measured absorbance, I_0 is the intensity of incident light at a given wavelength, I is the transmitted intensity. The intensity of the incident light I_0 is the sum of the intensities of transmitted, absorbed and reflected light.

$$I_0 = I_T + I_A + I_R$$

accordingly:

$$\frac{I_T}{I_0} + \frac{I_A}{I_0} + \frac{I_R}{I_0} = T + A + R = 1$$

Using this equation we have calculated the absorption as:

$$A = 1 - T - R$$

2.5.4 Grazing incidence X-ray diffraction analysis

With grazing incidence x-ray diffraction spectroscopy (GIXRD) structure profile of ZnPc absorber layer deposited on CuI and ITO substrates was examined.
In the essence of x-ray diffraction (XRD) spectroscopy stays the Bragg's law:

$$n\lambda = 2d\sin\theta$$

The lattice distance *d* is the distance between atomic layers in a crystal, and the variable λ is the wavelength of the incident x-ray beam; n is an integer. X-ray radiation has large penetration depth into any matter. Due to this fact conventional XRD is not surface sensitive analytic technique, and is appropriate for analysis of inorganic materials. Since we are dealing with thin organic films XRD with a grazing incidence angle is appropriate technique for structure analysis of our materials. In this method a monochromatic x-ray beam falls on a sample surface at fixed angle of incidence, thus the path length of the x-ray beam trough the film is increased and diffraction profile is recorded by detector only scan. With this arrangement of the XRD instrument the penetration depth of the x-rays is reduced by three orders of magnitude increasing the diffraction

intensity from the analyzed film.

2.5.5 Near edge x-ray absorption spectroscopy (NEXAFS)

With NEXAFS spectroscopy, molecular structure and orientation of phthalocyanine molecules deposited on ITO and CuI substrates was determined. Measurements were performed at the linear polarized ASTRID SX-700 beamline of ISA in Aarhus/Denmark with monochromator resolution r=0.88 eV. Molecular peak positions were determined from collected partial Auger electron emission data at the carbon K-edge.

NEXAFS monitors resonant electronic transitions from core levels of specific atomic species (C 1s, O 1s or N 1s) to unoccupied molecular orbitals or states (π^* and σ^* orbitals). Linearly polarized x-rays are best suited for covalent systems like macromolecules and polymers, which possess directional bonds. In this case the directional electric field vector of the x-rays can be viewed as a "search light" that can look for the direction of chemical bonds of the atom selected by its absorption edge. Phthalocyanines have unoccupied orbitals of σ and π symmetry which are oriented in and perpendicular to the ring plane, respectively. If the phthalocyanine molecule lies down on the substrate, when the electric field vector E is aligned along the surface normal, peaks due to the out-of-plane π orbitals are seen and when E is parallel to the surface resonances due to the in-plane σ orbitals are dominant. Therefore, the molecular orientation within a layer can be derived from the relationship between the resonant intensities and incident angle of light.

2.5.6 Electrical characterization of solar cells

For electrical characterization of our solar cells current-voltage characteristic measurements were carried out.

Analyses were performed at standard conditions on solar simulator with halogen and xenon lamps under one sun AM 1.5 illumination the following way: a voltage from –1 to +1 volts was applied on the electrodes of the cell and the flowing current was measured. The current was divided by the exact solar cell area, thus normalized to 1 cm^2 for easier comparison of the results. A typical J/V curve is shown in **Figure 13**.

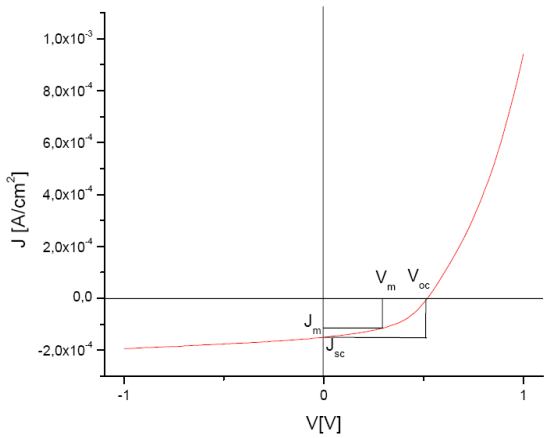

Figure 13. Typical Current/Voltage characteristic curve of a solar cell. V_{oc}-open circuit voltage, J_{sc} – short circuit current, V_m and J_m-voltage and current at the point of maximal cell power

Four device parameters can be determined from the electrical measurement: short circuit current density (J_{sc} [A/cm^2]), voltage (V [V]), fill factor (FF [%]) and power conversion efficiency (η [%]). J_{sc} is determined at the point where the applied voltage turns to zero (J/V curve overlies the Y axis). At this point the current, that is measured, is entirely current, yielded by the cell. The open circuit voltage – V_{oc}, is measured at the intersection of the J/V curve with X axis where the externally applied voltage equals the internal voltage of the cell, thus no current will flow. J_m and V_m are the current and voltage at the point where the maximum electrical power (P_{max}) of the cell is developed. Fill Factor (FF) is a solar cell characteristic depending on what extent the J/V curve fills the

rectangle outlined around its curvature in fourth quadrant. This shows how strong the J/V curve of the real cell deflects from the curve of an ideal diode. FF is calculated using the following equation:

$$FF = \frac{J_m \cdot V_m}{J_{sc} \cdot V_{oc}}$$

The power conversion efficiency of the solar cell - η, in percentages is calculated as follows:

$$\eta[\%] = \frac{P_{\max}}{P_{light}}.100 = \frac{FF \cdot J_{sc} \cdot V_{oc}}{P_{light}} \cdot 100$$

3. Results and discussion

3.1 Chemical engineering of TCO surface

In this chapter we apply the self synthesized functional phthalocyanine derivatives described in **2.3** on ITO in order to chemically modify its surface. Efficient buffer free organic solar cells with no electron traps and low energetic barrier at the inorganic-organic interface has been the main goal of the described work.

3.1.1 TCO work function modification

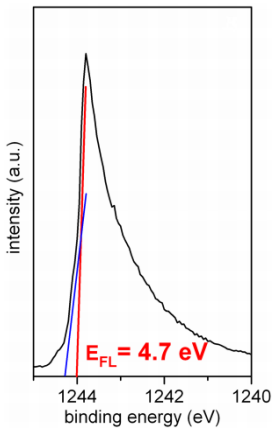

Figure 14. Work function XPS spectra of ITO substrate treated with SnPc axially substituted with gallic acid. The two-step profile indicates partial coverage by the treatment. Terminated ITO domains show increased work function (red), whereas nonterminated domains retain the original work function of ITO (blue).

Figure 14, shows low intensity XPS analysis of the work function of chemically modified ITO surface with SnPc axially substituted with gallic acid. On the Fermi energy (FE) edge we clearly observe two steps, indicating the presence of two different surface domains in the probed spot. Their positions were determined by linear fits corrected by the instruments resolution (+0.1 eV). On this spectrum the steps at higher binding energies (blue line) corresponds to a work function of 4.3 eV, which we assign to sputter-cleaned ITO [37]. The fit at lower binding energy step 4.7 eV (red line) corresponds to ITO passivated by the polar ligand of the termination molecule. The defined two work functions on one substrate indicate partial coverage by the TCO termination molecules. Since

the ITO termination was carried out by dip-coating the substrate in a solution of the active molecules (see **2.4.3**) the partial coverage could be explained with low solubility of the axial phthalocyanines. This result opened the question whether complete termination molecules are present on the ITO surface or only the ligand is attached there.

Near edge x-ray absorption fine structure spectroscopy (NEXAFS) was carried out on the same sort of substrates (**Figure 15**).

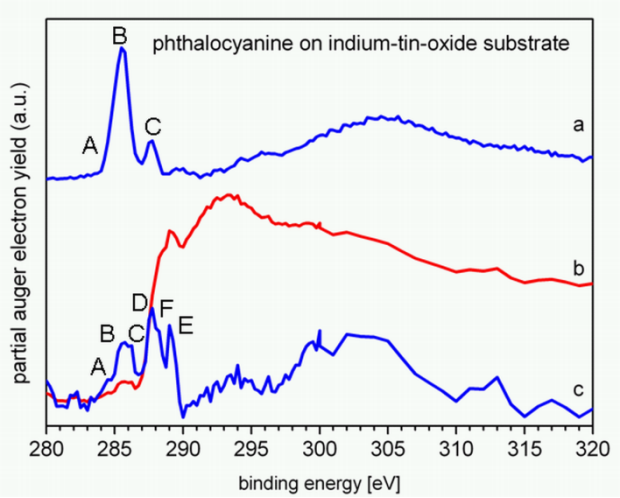

Figure 15. (a) Carbon K-edge NEXAFS reference spectra of ZnPc monolayers on SiOx, compared to (b) chemisorbed Sn-Pc axially substituted with gallic acid rest on ITO.(c) After subtraction of the carbon edge from (b), five weak molecular C1π→* peaks appear.

Figure 15b shows the carbon K-edge NEXAFS spectrum of Sn-phthalocyanine (SnPc) axially substituted with gallic acid rest chemisorbed on ITO. After subtraction of the carbon edge described by an error function with exponential decay, five weak peaks in the low-energy region appear corresponding to C1s→π* transitions (**Figure 15c**). In particular, peaks A and B (284,5 and 285.4 eV, respectively) are assigned to transitions in aromatic carbons of SnPc as well as gallic acid [38,39].

The peak C at 286.3 eV corresponds to the pyrrole heterocycle presents only in the SnPc [40]. Transitions A, B and C we also detect at similar positions in the reference spectrum of 2 monolayers ZnPc on SiOx substrates, **Figure15a**. Transitions D (287.66 eV) and E (289.2 eV) we assign to shake-up satellites of A and C, respectively [41]. The broad pattern of peak D indicates the presence

of an additional peak F from carboxylic group, the position of which is 288.2 eV according to ref. 40. This result proves the presence of a molecular monolayer termination on the ITO substrate.

3.1.2 J/V characterization of solar cells on terminated TCO

As it was already described in **1.4**, the hybrid interface between ITO and the first absorber layer in organic solar cells usually is adjusted by introducing an additional buffer layer. In this work we want to put stress on the production of buffer free organic solar cells. Using a new termination concept with functionalized absorber molecules we prepared photovoltaic devices where the hybrid interface is transformed into a band aligned π-π interface.

Figure 16 shows J/V curve of bilayer organic solar cell produced on terminated ITO, compared to a reference on untreated ITO.

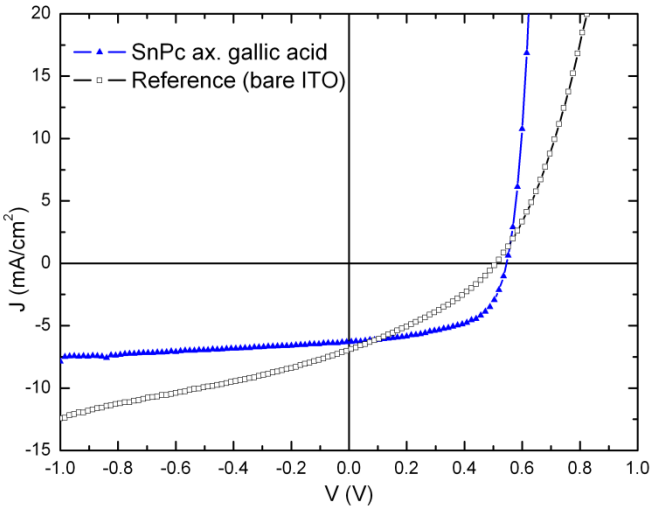

Figure 16. J/V characteristics of ZnPc/C_{60} bi-layer organic solar cells under one sun 1.5 AM illumination. The figure shows device produced on ITO chemically terminated with axially modified phthalocyanine in comparison with device on reference ITO.

Axially modified phthalocyanine applied as ITO terminating molecule yield solar cell with higher short circuit current densities (J_{sc}) of 6.3 mA/cm^2, due to much lower serial resistances R_s=0.5 Ωcm^2 compared to 9.8 Ωcm^2 of the reference device (Table 1). The parallel resistance under illumination is significantly increased to R_p=958 Ωcm^2 compared to R_p=163 Ωcm^2 for devices

produced on reference ITO. As expected the open circuit voltage with a value of 0.55 V was not significantly improved. Nevertheless the ITO termination biases higher fill factor (FF) 57% compared to 44% obtained with reference ITO. Likewise power conversion efficiency η is increased from 1.2 % up to 2.0 %. The reported improvement is related to the band alignment of the ITO Fermi energy to the ZnPc HOMO level, so that the energetic barrier at the hybrid interface is lower. This statement refers to the noted low R_s and high J_{sc} for devices produced on terminated ITO substrates. Furthermore the ITO termination forms an interface with lower trap barrier where less exciton recombination occurs. The lower voltage dependence of the light current under negative bias measured for the terminated ITO, i.e. the higher light R_p, is a strong hint for better charge extraction. The slightly increased V_{oc} indicates that the improved charge transport at the hybrid interface might diminish the space charge formed in the absorber layer reducing the charge carrier recombination at the D-A interface.

Sample	FE (eV)	J_{sc} (mA/cm^2)	V_{oc} (V)	FF (%)	η (%)	R_s (Ω*cm^2)	R_p (Ω*cm^2)
SnPc ax. gallic acid	4.7	6.3	0.55	57	2.0	0.5	958
ITO	4.3	5.2	0.51	44	1.2	9.8	163

Table 1. Device parameters of ITO/ZnPc/C60/Bathocuproine/Al OSC determined from J/V curves

The second phthalocyanine derivative prepared in three steps synthesis was also tested as ITO termination material, although the acetic functional group was not possible to be attached to the molecule. J/V curves measured from the device prepared on ITO terminated with 2,3,9,10,16,17,23,24 Octakis(octyloxy)phthalocyanine-iron (III) chloride compared to device on non coated ITO surface are presented in **Figure 17**. The investigated device shows lower J_{sc} which is probably due to disturbed charge transfer by the long octyloxy groups. But, these functional groups increased the solubility of the molecule in organic solvents and thus the homogeneity of the ITO coating layer. This state

was confirmed by the improved fill factor from 32% in the reference device to 46% for the device produced with coated ITO. However the efficiency was not influenced and showed similar value for both devices.

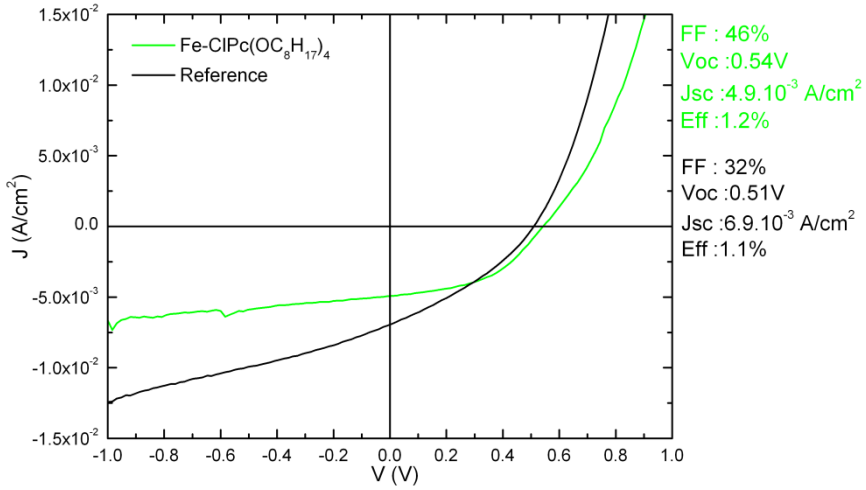

Figure 17. J/V curves and characteristic parameters of solar cells produced on terminated with 2,3,9,10,16,17,23,24 Octakis(octyloxy)phthalocyanine-iron (III) chloride compared to a reference device on only solvent cleaned ITO substrate.

In this chapter was demonstrated that the electronic properties of ITO surface can be chemically engineered using a TCO surface termination molecules. A monolayer of phthalocyanine molecules functionalyzed by the attached organic acetic group can be used instead of an additional buffer layer in phthalocyanine/C_{60} solar cells and thus the solar cell architecture can be simplified.

3.2 TCO morphology

3.2.1 Electrochemical growth of ZnO nanostructures

Various methods for the growth of ZnO nanorods, like chemical bath deposition, electrochemical deposition and vapor transport method can be found in literature. Typically the ZnO structures are prepared at high temperature of over 300 degrees centigrade. Most research with ZnO nanostructures (nanorods) for solar cell applications is reported for dye sensitized solar cells and polymer based solar cells. The dye sensitized devices allow nanostructures with several ten microns length, while for thin film polymer solar cells, length of less then 500 nm is required [22].

Here we prepare ZnO nanostructures by electrochemical deposition on two sorts of substrates. Commercial ITO substrate and commercial ITO covered with 10 nm layer of aluminum doped ZnO (AZO) prepared by sputter process. The preparation technique for the growth of ZnO nanostructures is reported by Dr. Jie Chen [42]. Here we further developed and specified the recipe for our substrates and for special size and packing density of ZnO nanostructures, so that they are appropriate for application in small molecule organic solar cell. The preparation starts with placement of the three electrode electrochemical cell (see **4.2.1 Figure 7**) in a thermoregulated bath. The temperature was adjusted to 75 °C. An aqueous solution of $Zn(NO_3)_2$ and HNO_3 with a mixture ratio of around 100:1 in molarities was used for deposition. The molarities of $Zn(NO_3)_2$ was 5 *mM*. Galvanic method with controlled current densities of 1.9 mA/cm^2 has been used for the electrochemical growth of nanorods on ITO. On AZO, rods are grown with controlled potential of -1.3 V versus Pt. In both preparations, solution was stirred during the deposition. The chemical reactions which occur at the working electrode during the electrochemical growth are the following:

$$Zn(NO_3)_2 \Leftrightarrow Zn^{2+} + 2NO_3^-$$
$$NO_3^- + H_2O + 2\,e^- \Rightarrow NO_2^- + 2OH^-$$
$$Zn^{2+} + 2OH^- \Leftrightarrow Zn(OH)_2$$
$$Zn(OH)_2 \Rightarrow ZnO + H_2O$$

First $Zn(NO_3)_2$ dissociate into Zn^{2+} and NO_3^- ions. Electroreduction of NO_3^- produces OH^- ions, which react with Zn^{2+} to form $Zn(OH)_2$ on the working electrode (ITO). The deposited $Zn(OH)_2$ decompose at about 70 ˚C to produce ZnO.

The deposition time was varied depending on the desired size of the nanostructures. The final product was washed with distilled water to remove any residual salt. The achieved morphologies with ZnO were imaged with scanning electron microscope (SEM), **Figure 18**.

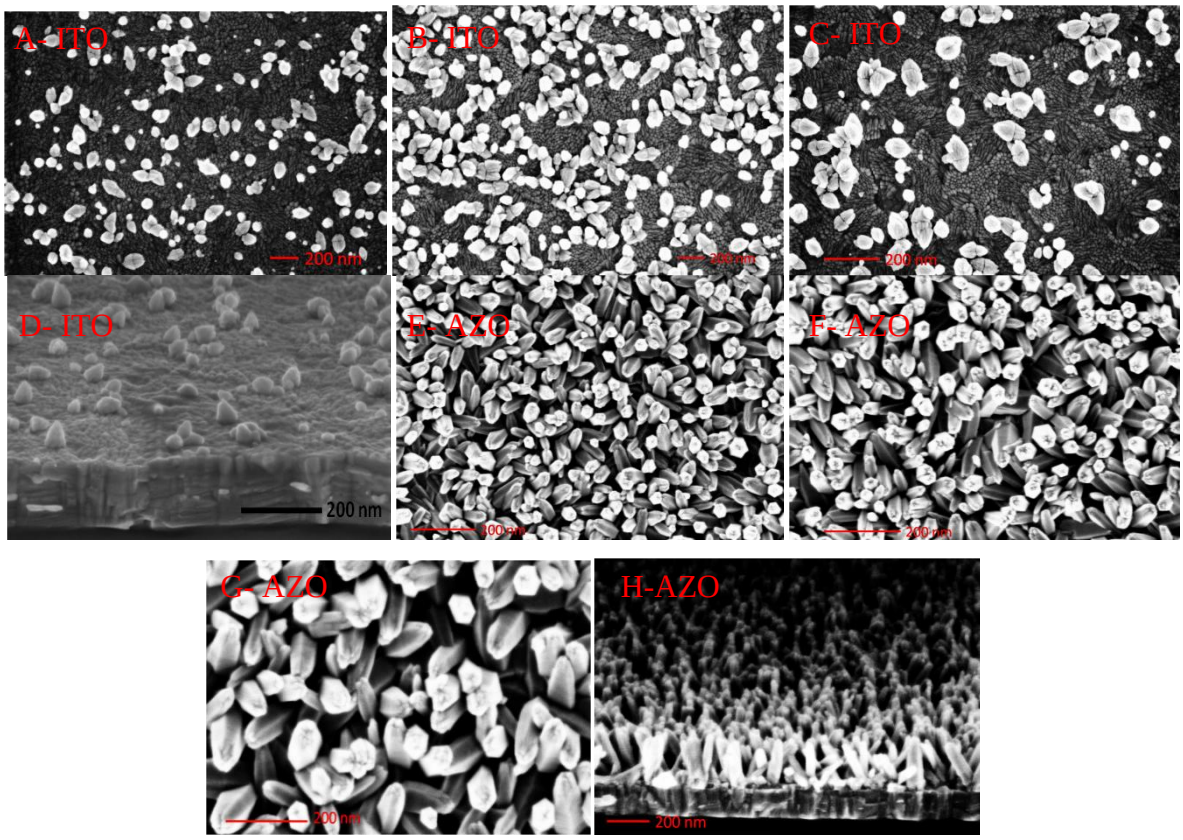

Figure 18. ZnO nanostructures prepared by electrochemical deposition on ITO at controlled current densities of 1.9 mA/cm^2. 50 to 80 nm , 80 to 100 nm and >100 nm structures are shown on images A, B and C. Cross section of one substrate with 50 nm ZnO is shown on image D. Images from E to G show ZnO nanorods with length of 50 nm, 100 nm and 150 nm, prepared at controlled potential of -1.3 V versus Pt on 10 nm aluminum doped ZnO layer (AZO) sputtered on ITO. Cross section image of ZnO nanorods with length of 200 nm on AZO is shown on image H.

As can be seen from the SEM images, ZnO nanostructures grow with rod like shape and higher packing density on sputtered AZO. AZO layer allows better control for the growth of ZnO nanorods. Nevertheless, we decided to study the optical effects of all prepared ZnO structures on both types of substrates, and to test them for organic solar cells.

3.2.2 UV-VIS spectroscopic studies

In order to study optical effects from the prepared ZnO nanostructures and to define their optimal size as substrate for organic solar cells, ultraviolet-visible spectroscopic study has been done. Zn-phthalocyanine (ZnPc) layers have been vacuum deposited on ZnO structures grown on ITO with 50-80 nm, 80-100 nm and >100 nm length and UV-VIS spectra in transmittance (T) and reflectance (R) modes are recorded. Absorption spectra of the same samples are calculated using the equation 1-T-R and presented in **Figure 19**. Where 1 is the total light. All spectra are normalized by thickness of ZnPc layer.

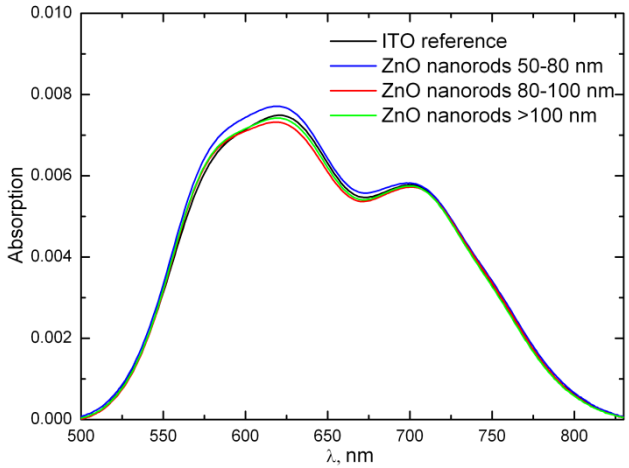

Figure 19. Absorption spectra of ZnPc deposited on ZnO structures with different length. Increased absorption is observed from the samples with 50-80nm ZnO.

The peak at 610 nm on the Q-band of ZnPc is a little bit stronger showing 3% higher absorption coefficient when this material is deposited on 50-80 nm long structures. On the other two substrates the ZnPc absorption is almost equal

compared to the reference. This result is attributed to light scattering by the substrates morphology. Instead of going straight trough the sample light is scattered in the ZnPc absorber material and thus absorbed with higher percentage. For samples with more than 80 nm morphology this optical effect is negligible.

Same study was carried out for samples with 50 nm, 100 nm and 150 nm ZnO nanorods prepared on AZO layer, **Figure 20**.

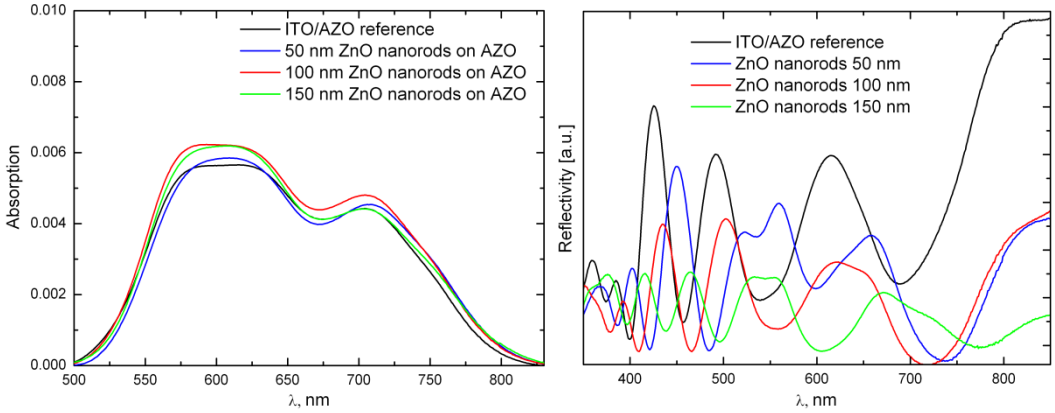

Figure 20. (Left) UV-VIS absorption spectra of ZnPc deposited on ZnO structures prepares on AZO with different length. 10% higher absorption is observed for the sample with 100 nm nanorods. (Right) Spectra recorded in reflectance modes for the same samples.

10% higher absorption was demonstrated by the sample with 100 nm nanorods compared to the reference sample on sputtered ITO. Similar spectrum showed the sample with 150 nm rods while on 50 nm ZnO the absorption spectrum of ZnPc is equal to that of the reference. When we looked also on the reflectivity spectra of the same samples (**Figure 20, Right**) we observed decreased reflectance in all samples with ZnO. Substrates with morphology reflect less light and thus more light is dispersed and absorbed by the ZnPc.

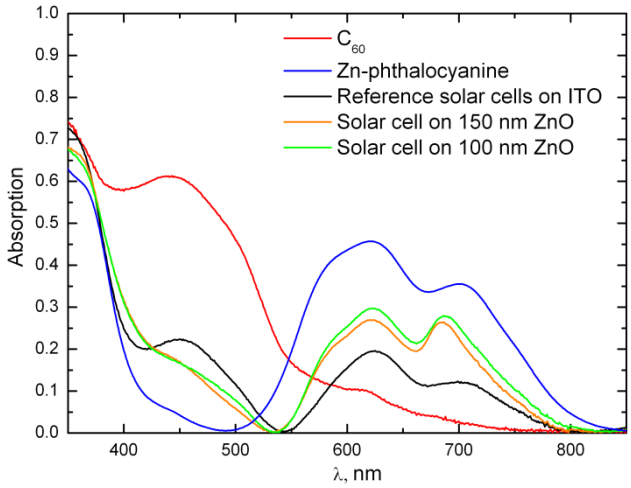

Figure 21. UV-VIS absorption spectra of OSC prepared on 100 nm and 150 nm ZnO nanorods deposited on AZO, compared to spectra from reference device on ITO. For comparison absorption spectra of single Zn-phthalocyanine (blue) and C60 (red) layers deposited on quarts are also presented in the graph.

On **Figure 21** we compared also absorption spectra of complete solar cells prepared on substrates with 100 nm and 150 nm long ZnO nanorods deposited on AZO to a reference cell fabricated on sputtered ITO. Here the optical effect from the substrates morphology is much stronger and the absorption in the device with 100 nm rods was improved with up to 35%, on account of decreased absorption peak at 450 nm from the C_{60} layer.

From our optical studies we can conclude that ZnO nanorods with 100 nm and 150 nm length prepared on AZO demonstrate the strongest optical effect and they are most promising morphological substrates for bi-layer organic solar cells.

3.2.3 Work function

Since we are going to introduce the ZnO nanostructures as alternative substrate for organic solar cells it is important to know their work functions and to understand how they fit in the energy diagram of the device.

Figure 22 shows low intensity XPS analysis of the work function of ZnO nanostructures prepared on ITO before and after chemical treatment with functional molecules. All spectra show a step on the Fermi energy edge speaking about two different domains in the probed spot. The step at 4.0 eV on the ITO+ZnO sample was attributed to the work function of ZnO while the step at 4.25 eV shows the work function of sputtered ITO [43]. After same substrate was chemically terminated with Sn-phthalocyanine axially substituted with gallic acid, phosphoric acid and peripherally substituted with phosphoric acid Zn-phthalocyanine [38] only the step related to the work function of ITO was shifted to 4.55 eV. This result clearly shows that ZnO prepared by electrochemical deposition is chemically inert. In contrast to the ITO its surface does not have open bindings (possible traps), which is in a good agreement with the requirements for the solar cell. The axially substituted phthalocyanine derivative which we synthesized can be used as selective passivation for ITO.

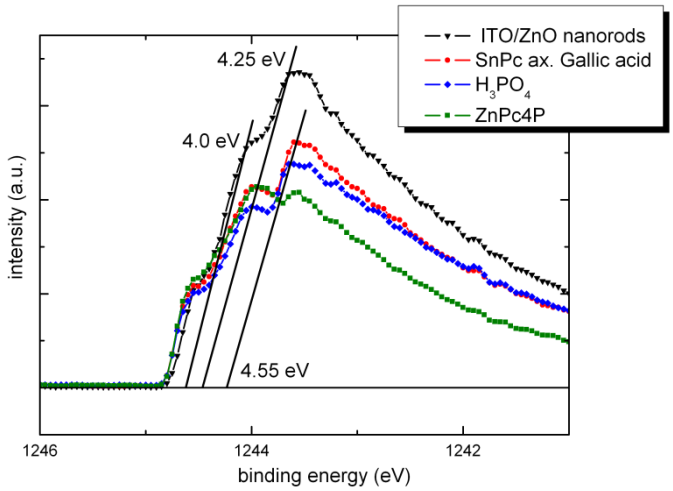

Figure 22. Work function XPS spectra of ZnO nanorods deposited on ITO by electrochemical deposition before and after chemical treatment with functional molecules as Sn-phthalocyanine axially substituted with gallic acid, phosphoric acid and peripherally substituted with phosphoric acid phthalocyanine. The two steps at 4.0 eV and 4.25 eV correspond to the work functions of ZnO and ITO, respectively.

3.2.4 J/V characterization of solar cells with ZnO structured TCO

In this study both substrates with ZnO prepared on ITO and on AZO are investigated as anode for OSCs. First, devices where the substrates are ZnO nanostructures grown on ITO have been produced. The size of the nanostructures was varied from 50 nm to >100 nm as it was done for the optical studies (see **Figure 19**). J/V curves and parameters of solar cells fabricated on these structures in one batch at same conditions are presented in **Figure 23** and compared to a reference device on sputtered ITO.

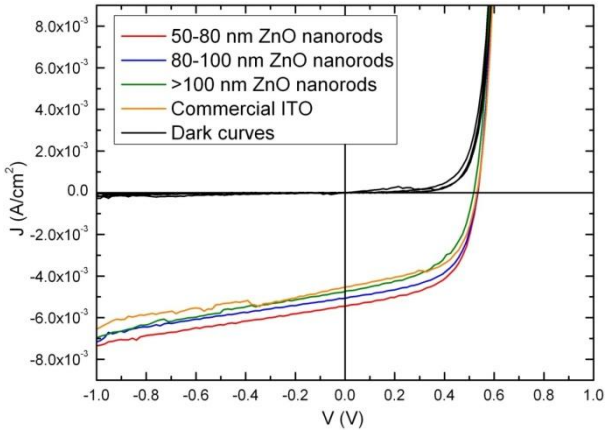

Solar cell parameters	FF (%)	V_{oc} (V)	$J_{sc}*10^{-3}$	Eff (%)
50-80 nm ZnO	57	0.53	5.4	1.65
80-100 nm ZnO	57	0.53	5.0	1.5
>100 nm ZnO	52	0.52	4.7	1.3
Commercial ITO	56	0.53	4.5	1.35

Figure 23. J/V curves and parameters of OSC prepared with ZnO nanorods with different length deposited on ITO compared to a device prepared on substrate without morphology.

Highest solar cells parameters were recorded for the device produced on 50-80 nm long nanostructures. The 20 % improved efficiency in this device compared to the reference is mainly due to more current flows. Fill factor (FF) is very slightly increased while the voltage remains the same value. From our optical studies for ZnO/ITO morphologies we already found that the ZnPc electron donor material absorb more light when is deposited on substrate with 50-80 nm ZnO. Referred to the device, this means that more

excitons are created in the ZnPc absorber layer, which is confirmed by the observed increased J_{sc}.

When the size of the nanostructures is increased to more than 100 nm all solar cells parameters have decreased values, which additionally confirms that, smaller structures (<100 nm) grown directly on ITO, are best for efficient device performance. Up to here we optimized the size of the ZnO structures when they are grown directly on ITO.

Same study was carried out also for solar cell produced on ZnO/AZO structures. The length of the nanorods was varied from 10 nm to 150 nm. Unfortunately only the solar cell on 10 nm ZnO showed J/V curve with diode behavior, **Figure 24 (left)**.

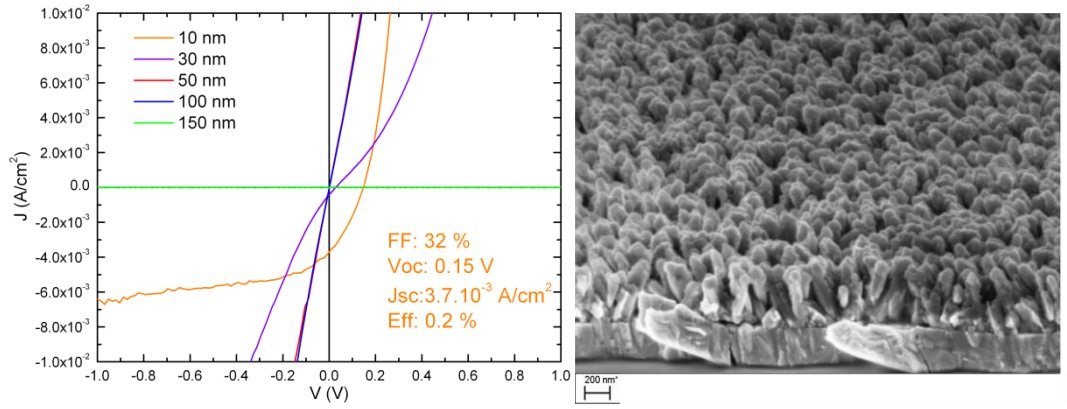

Figure 24 (Left) ZnO nanorods with length from 10 nm to 150 nm are grown on AZO and on top of them solar cells are produced. Their J/V curves show short cutted devices. Only the J/V curve of the solar cells on 10 nm ZnO shows a diode with very low efficiency. (Right) Cross section SEM image of solar cell fabricated on 100 nm ZnO nanorods. The organic layers do not cover completely the substrate allowing from and back contact of the device to be in contact.

All other solar cells showed short cuts, since the organic materials in the device do not cover completely the ZnO rods and thus the front and the back contact of the solar cell are in contact. This state was confirmed when we imaged a cross section of one device prepared on 100 nm nanorods with scanning electron microscope (SEM), **Figure 24 (right)**. From this image the unfilled with organic material gaps between the nanorods can be seen. With

thermal vacuum evaporation, materials are deposited only with perpendicularly oriented to the substrate deposition beam. This contributes to the incomplete covered with absorber rods.

In one additional experiment PEDOT:PSS was applied on the ZnO nanorods in order to isolate them from the back aluminum electrode. A thin layer of the polymer has been spin-coated on nanorods with different length. Devices are produced and their J/V curves measured in dark and under illumination were compared (**Figure 25**).

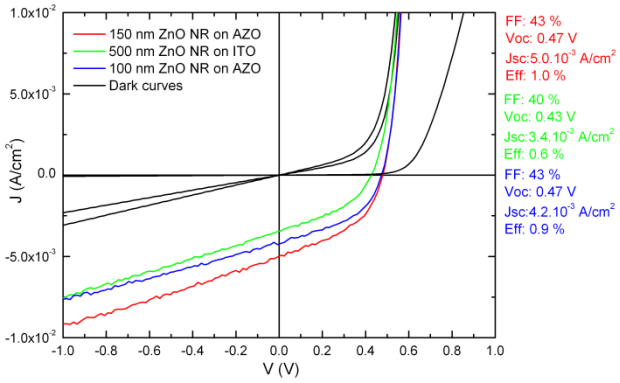

Figure 25. J/V curves and parameters of OSC prepared PEDOT:PSS covered 500 nm ZnO nanostructures grown electrochemically on ITO and 100 nm and 150 nm ZnO structures grown on AZO.

Devices produced on 100 nm and 150 nm structures showed curves with diode behavior and very similar device parameters. Efficient device was even produced on 500 nm ZnO structures. However the shape of all J/V curves at negative biases shows that there are still short cuts, which means that not all ZnO rods are covered by the polymer layer. Best coverage of the substrate is achieved in the device on 150 nm rods confirmed by the highest J_{sc} $5.0.10^{-3}$ A/cm^2 yielded in this device. This result demonstrates the potential of the ZnO nanorods prepared on AZO layer as anode for small molecule organic solar cells. After further investigations on the coverage of the nanorods, devices with higher power conversion efficiencies could be achieved.

As next step to enhance the coverage of the nanostructures with organic

material and to improve the device efficiency, wet chemical deposition of the first organic layer by spin-coating was held. Since phthalocyanines have low solubility in organic solvents we took the well know donor material from polymer solar cells Poly(3-hexylthiophen-2,5-diyl) (P3HT) [44]. After the polymer was dissolved in dichlorobenzene and spin coated on samples with and without ZnO structures, solar cells were produced. C_{60} was again used as electron acceptor material for these devices (**Figure 26**).

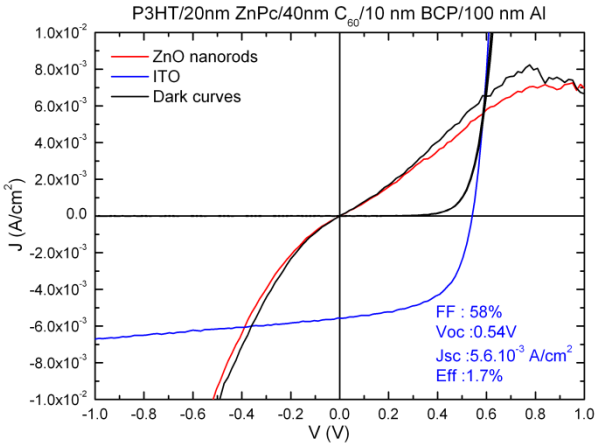

Figure 26. J/V curves of P3HT/C_{60} solar cell fabricated on ZnO nanorods compared to a reference device on sputtered ITO.

Unfortunately J/V curve of the device on ZnO structures showed short cuts. The cell on ITO demonstrated good parameters, but was not an object of this study.

In this chapter we have demonstrated second method to engineer the hybrid interface in OSC. Alternative TCO anode with defined morphology was developed and introduced in organic solar cells. Trough light scattering by the substrates morphology, the absorption of light in ZnPc layer was increased. Thus the power conversion efficiency of bilayer organic solar cells is raised with 20%.

3.3 TCO morphology-mesoporous ITO

In this chapter we modify the vacuum deposited ITO with mesoporous ITO prepared by sol-gel syntheses from molecular tin and indium precursors using block copolymer templates. We study the work function of the porous films and the morphology effect of the pores on the optical properties of the absorber material in the solar cell. In addition, we prepare devices and compare them to a reference with sputter deposited ITO.

3.3.1 Prepatarion of mesoporous ITO

Mesoporous ITO films with special 10 nm and 30 nm diameter of the pores have been prepared in the group of Prof. Bernd Smarsly, Institute of Physical Chemistry, Justus-Liebig-University Giessen with the following recipe [45].
Indium acetylacetonate (442 mg, 1 mmol) was dissolved in a mixture of 1.5 mL methanol and 1.5 mL acetone by careful heat treatment at 50 °C. After cooling for several minutes tin tetrachloride (30 mg, 0.1 mmol, 10 mol%) was added dropwise to the solution. As structure directing agent 70 mg (30 wt.% with respect to mass of ITO formed) PIB-PEO polymer were added and dissolved by ultrasonication. The resulting clear solution was used to produce thin films via dip-coating. Thin films were produced by casting commercial ITO substrates at low relative humidity (≤ 20%) into the precursor solutions and removing with defined speed (10 mms^{-1}) to give ca. 100 nm thin films. During evaporation of the solvent the polymers form micelles that undergo a self-organization process (evaporation-induced self-assembly, EISA process). After 2 min of drying, films were put into a furnace preheated to 80 °C for 1 h. Then they were heated to 300 °C within 4 h where they stayed for 12 h. Afterwards the films were heated quickly to 450 – 500 °C with a ramp of 10 °C per minute to induce crystallization (**Figure 27**).

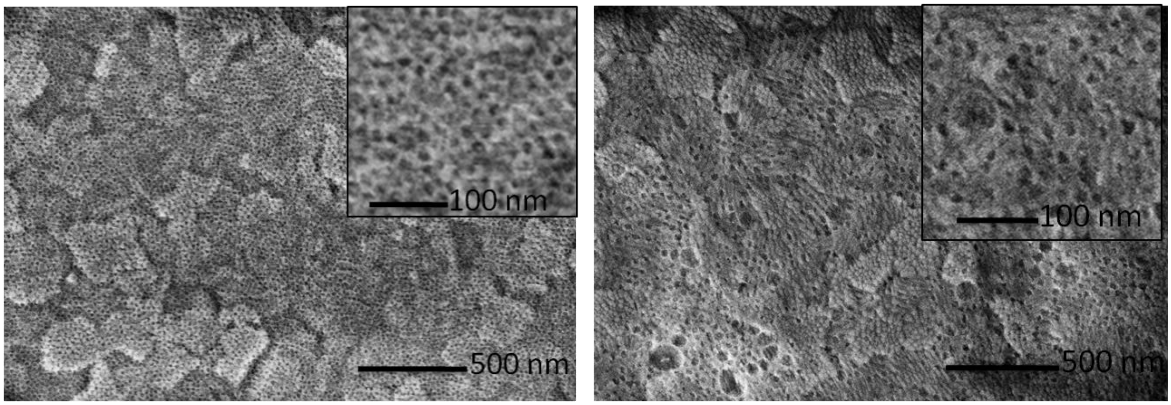

Figure 27. SEM images of mesoporous ITO with 10 nm pores (left) and 30 nm pores (right) prepared by dip-coating

The XRD patterns are in good accordance with literature values as can be seen in **Figure 28**. Applying the Scherrer equation leads to average crystallite sizes in the order of 14 nm for both types of mesoporous films.

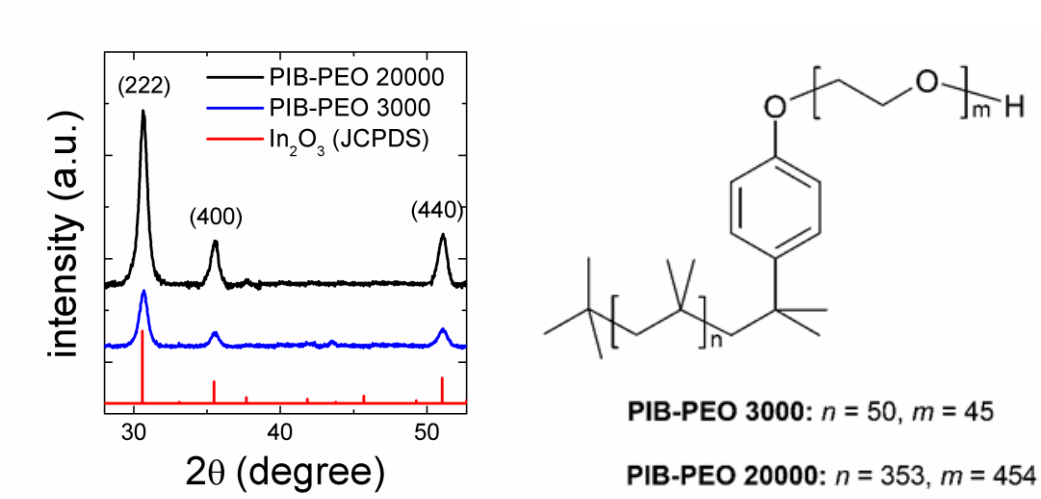

Figure 28. Left: XRD pattern of In2O3 taken from JCPDS *(00-006-0416)* and of ITO films templated with PIB-PEO 3000 or PIB-PEO 20000, respectively. Right: molecular formula of corresponding PIB-PEO templates.

3.3.2 Work function

Low intensity XPS analysis on the work function of solvent cleaned mesoporous ITO with 10 nm and 30 nm pores are shown on **Figure 29(A)**. Work function of 3.9 eV was determined for both substrates, independently of the pore size by a linear fit, corrected by the instrument resolution (+0.1 eV). Mesoporous ITO prepared by template-assisted sol-gel syntheses has lower work function than 4.3 eV of the sputter grown ITO. According to the energy level structure of the investigated devices, TCO anode with work function close to 5.2 eV is required. **Figure 29(B)** shows work function spectra of mesoporous ITO after it was dipped in a saturated solution of axially substituted with gallic acid Sn-phthalocyanine. Using the same molecule we successfully increased the work function of sputtered ITO from 4.3 eV to 4.7 eV [14]. In contrast, work function of mesoporous ITO (3.9 eV) remained unchanged. This result turned out to be reasonable, since published in literature surface analysis on the porous films show only scarce presence of hydroxyl (OH^-) groups [12]. The presence of these groups seems to be crucial for efficient surface reaction between the substrates and the acetic ligand of the organic molecules. Indeed, mesoporous ITO is a chemically stable material, with constant work function, which would contribute to production of devices with good reproducibility.

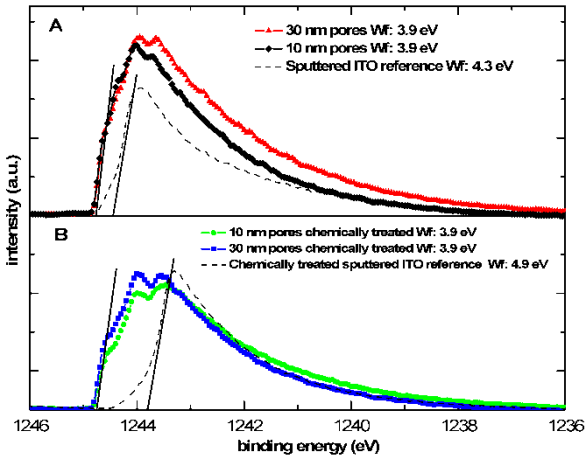

Figure 29. (A) Work function XPS spectra of mesoporous ITO substrates with 10 nm and 30 nm pores compared to sputter deposited ITO reference. (B) After chemical surface treatment with functionalized molecules, the mesoporous ITO retains its work function of 3.9 eV, while sputtered ITO showed a value as high as 4.9 eV.

3.3.3 Optical characterization (UV-VIS)

We have also investigated the influence of the porous ITO films on the optical properties of Zn-phthalocyanine. ZnPc was evaporated in vacuum on sol-gel processed mesoporous films with 10 nm and 30 nm pore diameter and on sputter grown ITO. Optical absorption spectra of the three samples recorded in the visible region are compared in **Figure 30**.

The two characteristic peaks for phthalocyanine at 610 nm and 705 nm have same position for all measured absorption spectra. Both spectra of phthalocyanine on mesoporous substrates show broader and stronger Q-band, compared to the reference. Highest absorption coefficient is recorded for the samples with 30 nm mesoporous ITO. These results demonstrate, that TCO films with larger pore diameter are more relevant for organic solar cells.

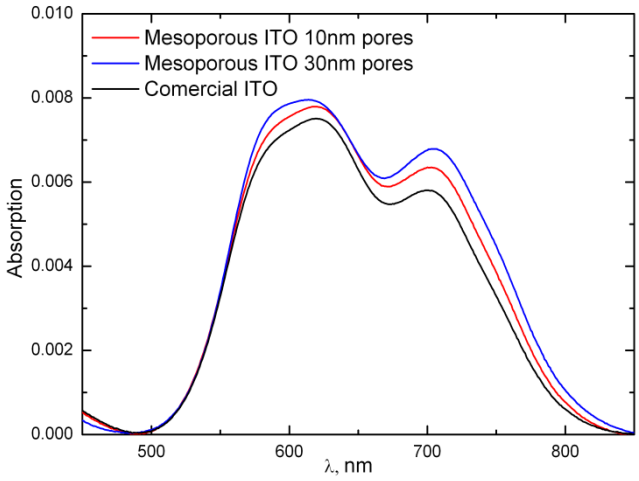

Figure 30. UV-VIS spectra of ZnPc deposited by thermal vacuum evaporation on mesoporous ITO. For comparison reference spectra of ZnPc on commercial ITO is also presented.

3.3.4 J/V characterization

We have examined both mesoporous ITO morphologies as substrates for OSCs. Devices were produced in one batch at same conditions. Their J/V curves and parameters are compared to that of a reference device on sputtered ITO and are shown on **Figure 31 and Table 2**.

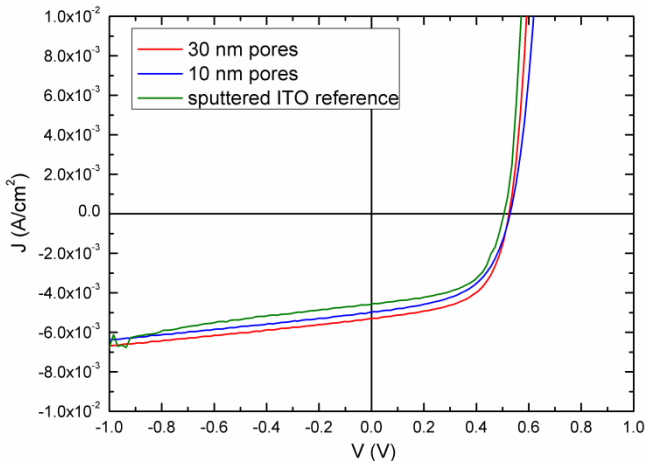

Figure 31. J/V characteristics of solar cells under one sun AM 1.5 illumination prepared on sol-gel processed mesoporous ITO with 10 nm and 30 nm pores, compared to a reference cell on sputtered ITO.

The highest power conversion efficiency η=1.6 eV is achieved by the device produced on mesoporous ITO with 30 nm pores (see Table 3). The investigated devices yield higher short circuit current densities (J_{sc}) of 5.3×10^{-3} and 5.0×10^{-3} A/cm^2 compared to 4.6×10^{-3} A/cm^2 of the reference. The open circuit voltage (V_{oc}) is slightly increased from 0.5 V in the reference cell to 0.53 V and 0.52 V in the cells prepared on 10 nm and 30 nm porous substrates, respectively. Nevertheless the fill factor of 57 % measured from the reference solar cell was not increased. However for the 10 nm pores substrate the fill factor dropped down to 54%.

The reported improvement in η of organic solar cells, prepared on mesoporous ITO substrates is related to scattered light in the absorber materials by the substrate morphology. This statement relies on the demonstrated higher $J_{sc.}$ The slightly increased V_{oc} in the range of the error bar speaks about improved exciton dissociation and possibly less recombination of charge carriers, probably due to increased active area at the organic-organic interface.

Solar cell parameters	FF (%)	V_{oc} (V)	J_{sc} x10^{-3} (A/cm^2)	η (%)
30 nm pores	57	0.52	5.3	1.6
10 nm pores	54	0.53	5.0	1.4
sputtered ITO ref.	57	0.50	4.6	1.3

Table 2. Summary of solar cell parameters determined from J/V curves at one sun AM 1.5 illuminations.

3.4 TCO morphology-ITO fibers

Crack-free mesoporous films with larger than 30 nm diameters of the pores was not possible to be prepared by template assisted sol-gel synthesis. In order to have substrate morphology with bigger porosity we decided to use ITO fibers. These structures were also prepared wet chemically in the group of Professor Bernd Smarsly in the frame of "SOHyb" project. Between the fibers, gaps with larger than 50 nm diameter are formed, **Figure 32**.

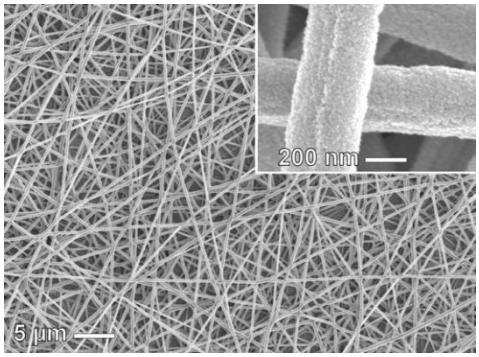

Figure 32. Top view of wet chemically prepared ITO fibers with scanning electron microscope.

3.4.1. Work function

As for the other two TCOs substrates that we have investigated as anodes in OSC we measured the work function of ITO fibers. Low intensity work function spectrum of ITO fibers can be seen on **Figure 33**.

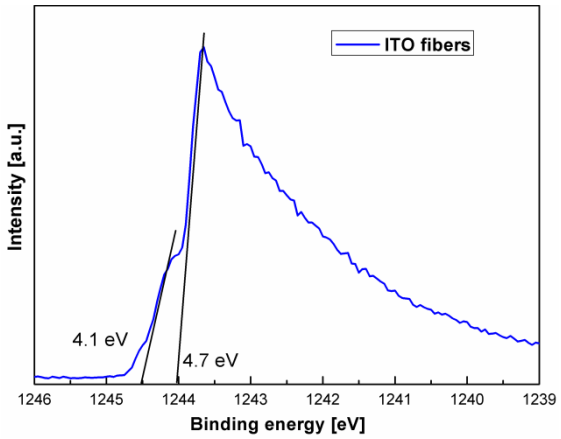

Figure 33. Low intercity work function XPS spectrum on ITO fibers. Two work functions are recognized on the Fermy energy edge. The one at 4.7 eV is that of ITO fibers. 4.2 eV is the work function of ITO used as substrate for the growth of the fibers.

There are two steps on the Fermy energy edge corresponding to two work functions. After two straight lines were fitted work function of 4.2 eV and 4.7 eV was found. The one at 4.2 eV we attribute to the sputtered ITO which is under the fibers, while 4.7 eV is the work function of the fibers. ITO fibers have the highest work function compared to all investigated TCOs in this thesis. If sputter deposited ITO is modified with these structures energetic barrier between the Fermi energy of TCO anode and the HOMO level of the ZnPc absorber can be reduced leading to fast charge extraction and less charge recombination at the inorganic-organic interface of the solar cell.

3.4.2 J/V characterization

Two solar cells on substrates with and without ITO fibers are fabricated and their J/V curves and parameters are compared on **Figure 34**.

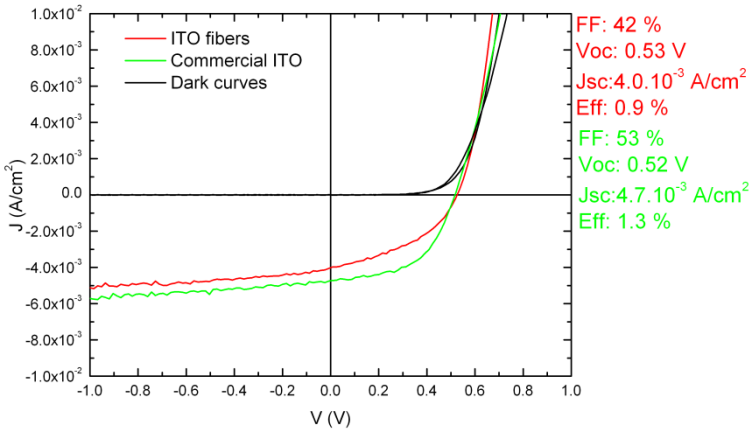

Figure 34. J/V curves and parameters of OSC prepared on ITO fibers, compared to device produced on commercial ITO.

Unfortunately the investigated device did not show better parameters than the reference. Here is important to be noted that this is one test device which is not optimized. This experiment demonstrates the potential of the ITO fibers as anode for OSCs. Due to time limitations further investigations on the ITO fibers was not possible to be done for this thesis. Further research can rely on layer thickness optimization, variation on size of ITO fibers, respectively diameter of holes between the fibers and variation of material deposition techniques, devices with better efficiency could be achieved.

3.5 TCO modification for oriented growth of absorber molecules

3.5.1 Structure analysis

By thermal vacuum evaporation two samples on flat glass substrates (100 Ω/cm^2) were prepared. One with 3 nm CuI (which we call template) and 30 nm ZnPc on top, and second with only 30 nm ZnPc. **Figure 35** shows the x- ray diffraction (XRD) pattern of ZnPc from these two samples.

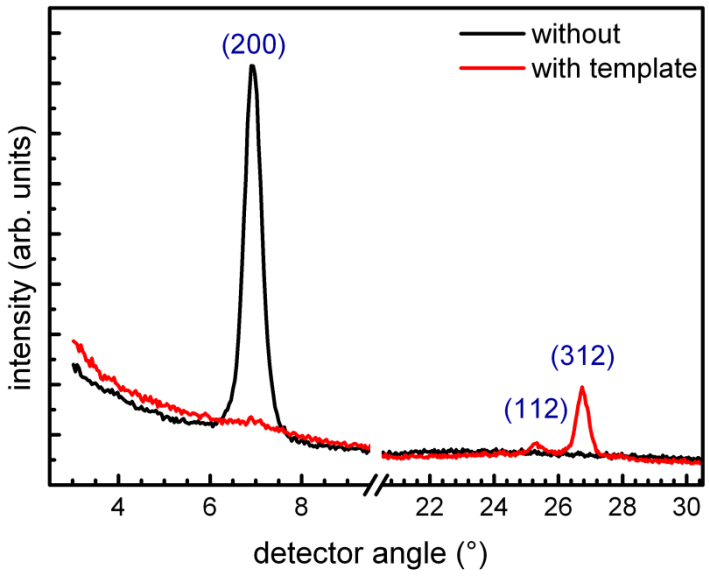

Figure 35. Grazing incidence XRD pattern of ZnPc deposited on CuI template, compared to that of non templated ZnPc.

Without CuI template, the XRD pattern shows a peak at 2θ = 6.9°, corresponding to the (200) Bragg reflection of the α- ZnPc phase [46,47]. For the sample with CuI template this peak disappears and a new peak at 2θ = 26.8° (312) occurs indicating that the stacking axis lies parallel to the substrate [48]. Since the molecule-molecule interactions between ZnPc molecules are same on both substrates, this change in the molecular orientation is attributed to substrate-molecules interactions.

Exemplary schematic draft on the molecular orientation of ZnPc on ITO and on CuI is presented on **Figure 36**.

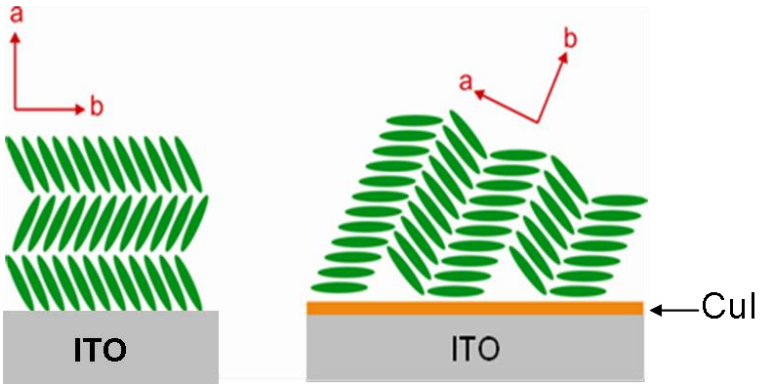

Figure 36. Schematic draft on the molecular orientation of ZnPc on ITO (left) and on 3 nm CuI layer deposited as template on ITO.

The XRD data clearly shows that the orientation of the ZnPc molecules is changed, but we are still uncertain about the tilt angle of the molecules. To clarify that near edge x-ray absorption fine structure spectroscopy (NEXAFS) was performed.

3.5.2 NEXAFS study on the molecular orientation of ZnPc

Thin film 5 nm of ZnPc has been prepared by thermal vacuum evaporation on ITO substrate covered with 3 nm CuI. The orientation of the molecules within the film is investigated by probing the intensity of the NEXAFS π and σ resonances as a function of the polarization vector of the light. In this case the focus is on the π orbitals which are perpendicular to the plane of the molecule.
On **Figure 37 (left)** the angular dependent C k-edge spectra of ZnPc are shown. The π* feature are enhanced for big angle of incidence indicating that the molecules lay close to parallel to the surface. The calculated intensity ratios of π*-orbital vector as the function of its tilt angle α with respect to the surface normal and the x-ray incidence angle θ are shown on **Figure 37 (right)**. The best fit for 5 nm ZnPc layer on CuI shows an average molecular tilt angle of 45° with respect to the substrate surface.

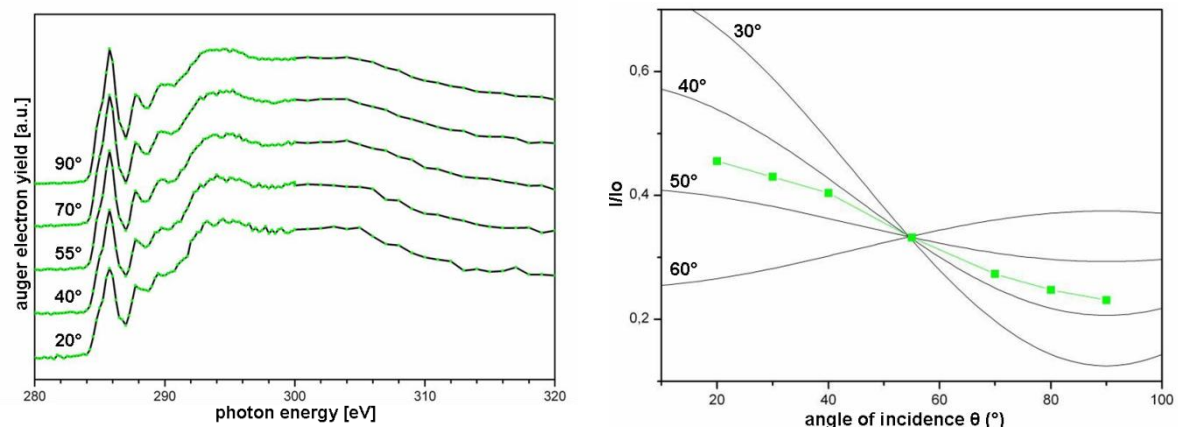

Figure 37. Left: NEXAFS spectra at the C k-edge of 5 nm Zn-phthalocyanine deposited on 3 nm CuI layer. Right: Evaluation of the π* peak intensity versus the angle of incidence. The average molecular tilt angle of ZnPc on CuI is found to be 45°.

3.5.3 Optical studies

To study the effect of the changed molecular orientation on the light absorption in the ZnPc layer, UV-VIS spectroscopy has been carried out. **Figure 38** shows the optical absorption spectra of glass/CuI/ZnPc (red) and glass/ZnPc (blue) samples. Both spectra are normalized by the layer thickness of the deposited material.

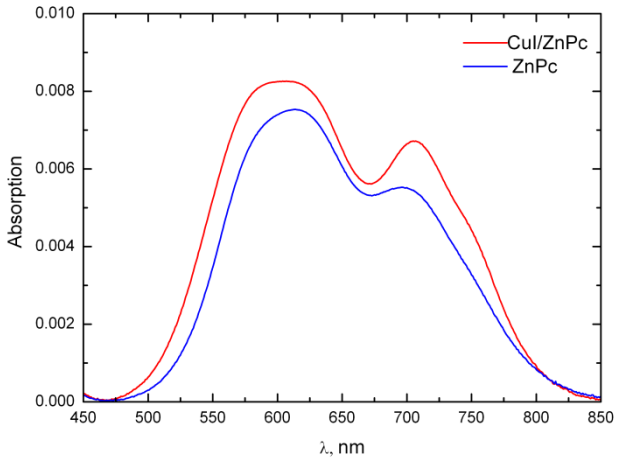

Figure 38. Q-band UV-VIS spectra of ZnPc deposited on CuI template and on ITO substrate.

On the Q (π-π* transition) characteristic band of phthalocyanine two peaks are observed. For the sample without CuI the peaks maxima are located at the wavelength of 610 nm and 700 nm, which is typical for ZnPc films. When a 3 nm layer of CuI was used as template for oriented growth of the ZnPc molecules the Q band became broader and stronger. The two peak maxima showed 10 nm

blue and red shifts to 600 nm and 710 nm, respectively. The absorption intensity of the Q band increases with 30% by inserting CuI template layer.

In one additional experiment the thicknesses of the ZnPc layer was varied from 5 nm to 90 nm while the thickness of the CuI layer was kept constant, i.e. 3 nm. 60 nm ZnPc deposited on ITO was taken as a reference sample. **Figure 39** shows the optical absorption spectra of all measured samples.

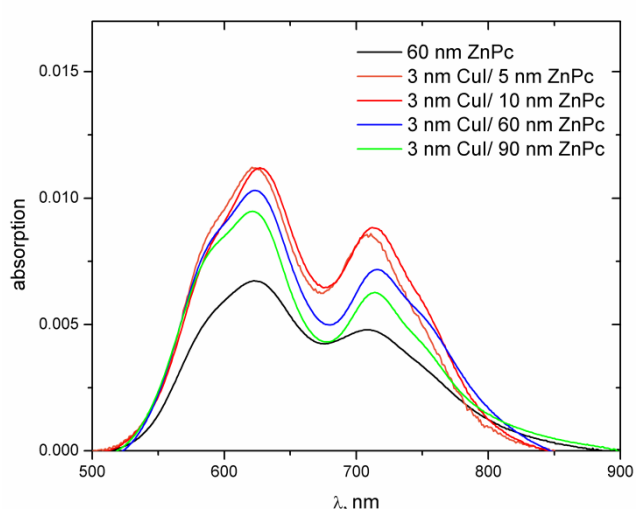

Figure 39. Optical absorption spectra of 60 nm Zn-phthalocyanine deposited ITO for a reference sample and Zn-phthalocyanine deposited on 3 nm CuI with layer variable thickness from 5 nm to 90 nm.

The α-phase of phthalocyanine shows two absorption maxima located at wavelengths of 625 nm and 710 nm. When the phthalocyanine molecules are reoriented toward the direction of the polarizing light they absorb at the same position in the visible part of the spectrum but with up to 66% higher absorption coefficient than the reference for 5 nm and 10 nm layers. Lower absorption coefficients but still higher than the reference are observed in 60 nm and 90 nm layers. This result gives us a hint that, when we increase the phthalocyanine layer thickness to more than 10 nm the molecules pass from parallel to upright standing orientation with respect to the substrate surface. For 5 nm and 10 nm layers most molecules are parallel oriented to the substrate. While at 60 nm and 90 nm layers most of the molecules are upright standing, even those in the first nanometers, and only one fraction molecules have parallel orientation. This fraction reoriented molecules contribute to the increased absorption coefficients

of these two samples compared to the reference.

3.5.4 Work function of CuI and molecular orientation of ZnPc

Work function of 3 nm CuI deposited on ITO was also measured with XPS. As expected high work function of 5.5±0.1 eV was determined for this material after a linear fit was done on the Fermi energy edge, **Figure 40**.

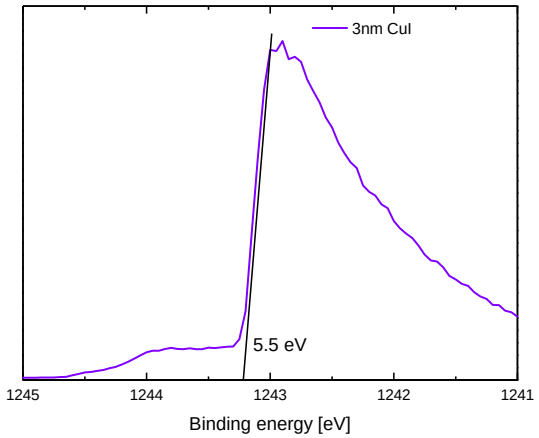

Figure 40. Work function spectrum of deposited on ITO substrate copper iodide. The work function of CuI is 5.5 eV. Information from the substrate formed a step on the edge at about 4.3 eV.

The small step at higher energies is engendered by slower electrons exited from the ITO substrate. The work function of CuI fits well to the band structure of the electron donor material in our device, so if we modify the TCO anode with this material the energetic barrier for hole extraction at the front side of the cell could be reduced.

Up to here, from our investigations with CuI we have seen that phthalocyanines deposited on this material change their molecular orientation. But what is still unclear is whether the molecular orientation is same for different layer thickness of the phthalocyanine. We wanted to clarify this point in one simple study with XPS.

On ITO substrate we have deposited 3 nm CuI and on top of it ZnPc layer with thickness 1.5 nm, 3 nm, 5 nm and 10 nm. Then their work functions were measured. Results are shown on **Figure 41 (A,B,C,D)**.

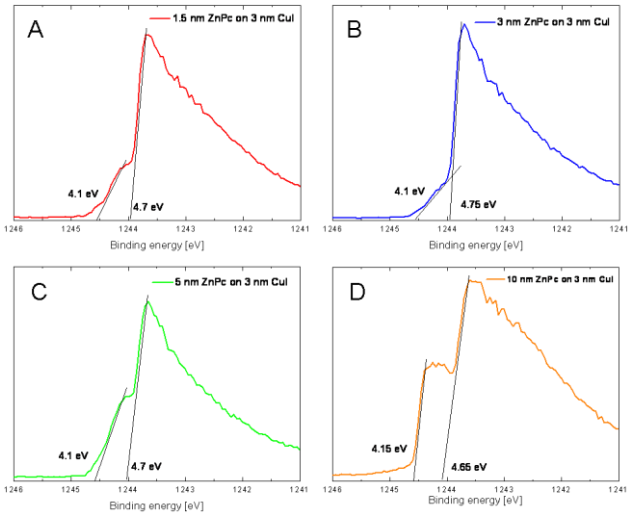

Figure 41. Work function spectra of ZnPc deposited on 3 nm CuI with layer thickness 1.5 nm (A), 3 nm (B), 5 nm (C) and 10 nm (D). Two work functions are recognized on every sample. The one at 4.1 eV corresponds to perpendicularly oriented molecules with respect to the substrate surface, while 4.7 eV ± 0.5 is the work function of parallel oriented molecules.

In all spectra two steps on the Fermi energy edge are observed, corresponding to two work functions on one sample. The step at 4.1 eV shows the work function of α phthalocyanine with upright standing orientation of the molecules toward the substrate. This value is in agreement with the published in literature values [49]. The step at about 4.7 ±0.5 eV we attribute to the work function of flat laying phthalocyanine molecules. The step height on the edge corresponds to the fraction of phthalocyanine molecules with one orientation at the expense of the other. For 3 nm phthalocyanine layers (**Figure 41, B**) almost all molecules are lying flat on the substrate. There is a little bit more upright standing molecules in the 1.5 nm layer (**A**), while in 5 nm (**C**) and 10 nm (**D**) layers 50 % of the molecules are laying flat and 50 % are upright standing. Here we can conclude that when we increase the thickness of the organic layer the molecules pass from flat lying configuration to upright standing configuration which is due to weakening of the substrate-molecule interactions. Note that, this result is in good agreement with the earlier results on the absorption coefficients of ZnPc for different thickness of its layers (see **3.5.3** and **figure 39**). Besides, the model we build for the molecular orientation of 30 nm ZnPc layer after we performed XRD study is additionally confirmed (see **figure 35**).

3.5.5 Solar cell preparation and characterization

Seeing all positive effects of CuI on the material properties of phthalocyanines, we were interested also to study its effects on the device performance. Two types of devices were fabricated. For one device we have deposited 3 nm CuI on ITO in order to control the molecular ordering of the ZnPc electron donor molecules and to modify the TCO anode. Reference device without CuI was prepared for comparison. The J/V curves and parameters of the two are presented on **Figure 42**.

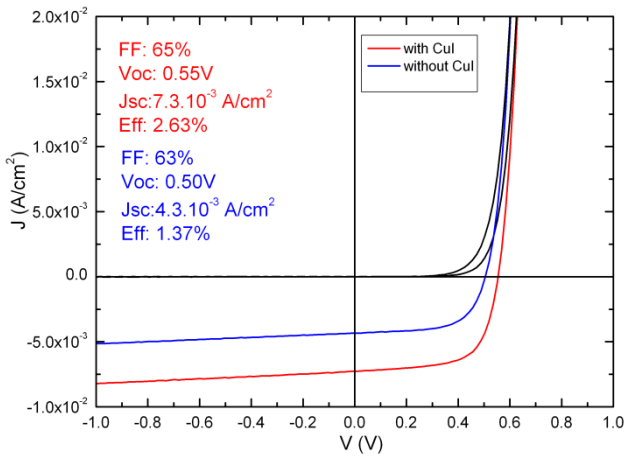

Figure 42. J/V characteristics of ZnPc/C60 OSCs prepared with and without CuI template for oriented growth of the ZnPc molecules.

Bilayer OSC with record efficiency for this work of 2.6 % was produced. All parameters of the device on CuI show higher values than that of the reference device. The 30 % increased absorption coefficient of the electron donor material resulted in 70% improved $J_{sc,}$ from $4.3.10^{-3}$ A/cm^2 to $7.3.10^{-3}$ A/cm^2. Furthermore, the new stacking orientation of the phthalocyanines provided larger carrier mobility for this material confirmed by the increased both J_{sc} and V_{oc} (from 0.5 V to 0.55 V). With CuI an interface with no energetic barrier was achieved allowing smooth charge extraction to the front electrode of the device which positively influenced the same two parameters. Fill factor was slightly enhanced from 63 % to 65 %.

In one last study we have compared all three molecules we have used to

chemically engineer the hybrid interface in OSCs. In one batch at same preparation conditions we have produced device whose TCO was modified with SnPc axially substituted with gallic acid, 2,3,9,10,16,17,23,24 Octakis(octyloxy)phthalocyanine-iron (III) chloride and CuI. Their parameters and J/V curves were compared to a reference with only solvent cleaned bare ITO, **Figure 43**.

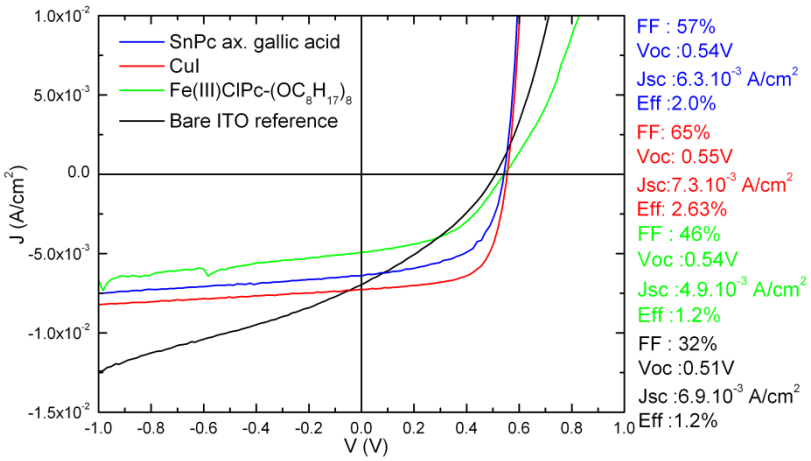

Figure 43. Comparison of J/V characteristics and parameters of OSCs prepared on TCO terminated with different molecules.

All devices show good reproducibility which describes them as industrially relevant. Using both, axially substituted phthalocyanines and CuI, we have successfully engineered the hybrid interface in bilayer OSCs made from small molecules, raising more than double their power conversion efficiency. So far, the highest power conversion efficiency of 3.6 % for planar heterojunction solar cells with only two active layers is reported by Peumans *et al.* [50]. The solar cells have the following architecture: ITO/PEDOT:PSS/CuPc/C_{60}/BCP/Al. In this work we succeeded to produce PEDOT:PSS free organic solar cells with similar efficiency, simplifying the device architecture. Heaving in mind, that OSCs must be cheap, easy and fast in production, we produced devices with one process less. In the last years much higher efficiencies have been reported for OSCs, but for devices with complicated concepts, on larger areas and with long production process. Usage of organic dopants, [51] metal nanoprticle dopants,

[52] staked tandem solar cells architectures [53] and p-i-n architectures [54] are some of the strategies that have been used to increase efficiencies. Efficiency of p-i-n solar cells from small molecules reached 3.7% [55]. By doping rubrene with CuPc, Chen *et al*. reported 5.58 % efficient devices. But, today most efficient are the stacked tandem cells with mixed layers of polymers and small molecules. In April 2012 the German company "Heliatek" certified 10.7% efficient tandem solar cell on 1.1 cm^2 area, setting the new world record in thin film OSCs [56]. Just a month later the record was beaten by "Mitsubishi Chemical Corp." with 11 % efficient tandem device [57].

4 Summary

Bilayer heterojunction organic solar cells (OSCs) consisting of Zn-phthalocyanine (ZnPc) as electron donor and fullerene (C_{60}) as electron acceptor material were optimized in this thesis. The research was focused on the chemistry and morphology of the hybrid interface between the transparent conductive oxide (TCO) anode, in the particular case indium-tin oxide (ITO) and the first organic layer ZnPc. Three approaches were pursued:

1. The interface was chemically engineered by simple dip-coating techniques that terminate ITO prior to ZnPc absorber deposition with synthesized novel axially substituted metal-phthalocyanine molecules. From collected near edge x-ray fine structure spectroscopy (NEXAFS) data the presence of a molecular monolayer termination on the ITO substrate was proved. Photovoltaic devices were prepared using vacuum thermal deposition techniques and applying the new termination concept with modified absorber molecules. Thus the hybrid interface was transformed into a band aligned π-π interface with improved transport properties yielding 2.0 % power conversion efficiency η, with 67% higher than the reference device.

2. As another approach TCO substrates with morphology were investigated for organic solar cell applications. ZnO nanostructures with different length were electrochemically grown on commercial ITO. Additionally, mesoporous ITO with specific pores of 10 nm and 30 nm was examined. Due to light scattering ZnPc absorber deposited on those morphological substrates absorbed up to 20 % more light. Transferred to the device, this effect enhanced short circuit current density (J_{sc}) by up to 17 %. Efficiency of devices with both morphologies reached 1.6 %.

3. Moreover, in the present dissertation CuI was introduced on ITO as template for oriented growth of the absorber molecules. Analysis on the NEXAFS structure profile of ZnPc films showed decreased molecular tilt angle from 70° on non-templated substrate to 45° on CuI template. With that molecular rearrangement ZnPc absorber layer had 30 % higher absorption coefficient than in conventional α-phase film structure. Bilayer devices produced on 0.032 cm^2 active area yielded J_{sc} as high as 7.3 A/cm^2 and 65 % fill factor, thus record efficiency of 2.6 % was achieved.

Zusammenfassung

In dieser Dissertation wurden organische Zweischichtsolarzellen mit einem Heterokontakt bestehend aus Zink-Phthalocyanin (ZnPc) als Elektronendonator- und Fulleren (C_{60}) als Elektronenakzeptormaterial optimiert. Im Vordergrund der Forschung stand dabei die Hybrid-Grenzfläche zwischen der Elektrode aus einem transparenten leitfähigen Oxid (TCO), hier Indium-Zinnoxid (ITO), und der ersten organischen Absorberschicht aus ZnPc. Drei Ansätze wurden verfolgt:

1. Die Grenzfläche wurde durch einfaches Tauchbeschichten chemisch angepasst. Dabei wurde das ITO vor Deposition des ZnPc Absorbers mit neuen synthetisierten axial substituierten Metall-Phthalocyaninmolekülen terminiert. Dass die molekulare Monolage auf dem ITO Substrat vorhanden ist, konnte mit Röntgen-Nahkanten-Absorptions-Spektroskopie (NEXAFS) bewiesen werden. Solarzellen wurden unter Verwendung thermischer Vakuumdeposition und dem neuen Konzept der Terminierung mit modifizierten Absorbermolekülen hergestellt. Damit wurde die Hybridgrenzfläche in eine bandangepasste π-π Grenzfläche mit verbesserten Transportfähigkeiten umgewandelt womit ein Wirkungsgrad η von 2% Wirkungsgrad erreicht wurde, der 67% höher ist als für die Referenzzelle.

2. Als weiterer Ansatz wurden TCO Substrate mit nanostrukturierter Morphologie für die Anwendung in organischen Solarzellen untersucht. ZnO Nanostrukturen mit verschiedenen Längen wurden elektrochemisch auf kommerzielle ITO Substrate deponiert. Zusätzlich wurde mesoporöses ITO mit spezifischen Porengrößen von 10 und 30 nm untersucht. Austrittsarbeiten von 3,9 eV für ZnO und 4,0 eV für mesoporöses ITO wurden unabhängig von der Größe der Nanostrukturen gemessen. Auf Grund von Lichtstreuung absorbierten ZnPc Schichten, die auf solche strukturierten Substrate deponiert wurden, bis zu 20% mehr Licht. In Solarzellen führte dieser Effekt zu einer 17% höheren Kurzschlussstromdichte (J_{SC}). Mit beiden Morphologien wurden Wirkungsgrade von 1,6% erreicht.

3. In der vorliegenden Dissertation wurde außerdem CuI auf ITO als Unterlage für ein orientiertes Wachstum der Absorbermoleküle eingeführt. Die Analyse des NEXAFS Strukturprofils von ZnPc zeigte einen Kippwinkel, der sich von 70° für Substrate ohne CuI auf 45° mit CuI verringerte. Mit dieser molekularen Umordnung wurde für die ZnPc Schicht ein 30% höherer Absorptionskoeffizient erzielt als mit der konventionellen α-Phasen-Filmstruktur. Zweischichtsolarzellen mit einer aktiven Zellfläche von 0,032 cm^2 erreichten eine typische J_{SC} von 7,3 mA/cm^2, einen Füllfaktor von 65% und damit einen Rekordwirkungsgrad von 2,6%.

5 Literature and References

[1] Birol F. (eds.), World Energy Outlook (2004).

[2] A. Shah, P. Torres, R. Tscharner, N. Wyrsch, H. Keppner, Science 285, 5428, (1999), 692.

[3] E. Bequerel, C. R. Acad. Sci. (1839), 9, 145.

[4] Christoph J. Brabec, Solar Energy Materials & Solar Cells 83, (2004) 273–292.

[5] Martin A. Green, J Mater Sci: Mater Electron (2007).

[6] G.A. Chamberlain: Organic solar cells: A review. Solar Cells 8, 47, (1983).

[7] D. L. Morel, A. K. Gosh, T. Feng, E. L. Stogryn, P. E. Purwin, R. F. Shaw, and C. Fishman, Appl. Phys. Lett. 32, 495, (1978).

[8] C. W. Tang, Appl. Phys. Lett., Vol. 48 No.2 (1986) 183-185.

[9] G. Chidichimo and L. Filippelli, International Journal of Photoenergy, Volume (2010).

[10] Harald Hoppe and Niyazi Serdar Sariciftci, J. Mater. Res., 19, 7, (2004).

[11] C. D. Dimitrakopoulos and D. J. Mascaro: Organic thin-film transistors: A review of recent advances. IBM J. Res. Dev. 45, (2001).

[12] C. Weisbuch, H. Benisty, R. Houdbrè, Journal of Luminescence, 85 (2000) 271-293.

[13] Peumans, S. Forrest, Chem. Phys. Lett., 398 (2004) 27-31.

[14] K. Coakley, M. McGehee, J. Chem. Mater., (2004).

[15] D. Zheng, Z. Gao, X. He, F. Zhang, L. Liu, Applied Surface Science 211 (2003) 24–30.

[16] G. Greczynski, Th. Kugler, M. Keil, W. Osikowich, M. Fahlman, W. Salaneck, Journal of Electron Spectroscopy, 121 (2001) 1-17.

[17] P. Schilinsky, C. Waldauf, Appl. Phys. Lett. 80, (2002) 3885.

[18] Xi Xi, Qinglei Meng, Fangxin Li, Yuqiang Ding, Jingjia Ji, Zhengrong Shi,

Guohua Li, Solar Energy Materials & Solar Cells 94, (2010) 623-628.

[19] Mikkel Jorgensen, Kion Norrman, Frederik C. Krebs, Solar Energy Materials & Solar Cells 92, (2008) 686- 714.

[20] Jiao Li, Juncheng Liu, Congjie Gao and Guohua Chen, International Journal of Photoenergy, 2011, (2010).

[21] T. Aernouts, W. Geens, J. Poortmans, P. Heremans, S. Borghs, R. Mertens, Thin Solid Films, 403-404 (2002) 297-301.

[22]Janos Sartor, F. Maier-Flaig, J. Conradt1, J. Fallert, H. Kalt, D. Weissenberger, and D. Gerthsen, P hys. Status Solidi C 7, 6, (2010) 1583– 1585.

[23] C. D. Dimitrakopoulos and P. R. L. Malenfant, Adv. Mater. 14, (2002), 99.

[24] F. Garnier, A. Yasser, R. Hajlaui, G. Horowitz, F. Deloffre, B. Servet, S. Ries, and P. Alnot, J. Am. Chem. Soc. 115, (1993), 8716.

[25] P. Sullivan, T. S. Jonesa, A. J. Ferguson, and S. Heutz, Appl. Phys. Lett. 91, (2007), 233114.

[26] J. Y. Lee, S. Roth, and Y. W. Park, Appl. Phys. Lett. 88, (2006), 252106.

[27] V. Coropceanu, J. Cornil, D. A. S. Filho, Y. Olivier, R. Silbey, and J.-L. Brédas, Chem. Rev. 107, (2007), 926.

[28] Y. Kinoshita, R. Takenaka, and H. Murataa, Appl. Phys. Lett. 92, (2008).

[29] V. Shrotriya, G. Li, Y. Yao, C. W. Chu, and Y. Yang, Appl. Phys. Lett. 88, (2006).

[30] D. W. Zhao, X. W. Sun, C. Y. Jiang, A. K. K. Kyaw, G. Q. Lo, and D. L. Kwong, Appl. Phys. Lett. 93, (2008).

[31] P.M. Sirimanne, M. Rusop, T. Shirata, T. Soga, T. Jimbo, Materials Chemistry and Physics 80 (2003) 461–465.

[32] J. F. van der Pol, E. Neeleman, J. W. Zwikker, R. J. M. Nolte and W. Drenth, Recl. Trav. Chim. Pays-Bas 107, (1988), 615-620.

[33] Kaifer, A. E. and Gomes-Kaifer, M. Wiley-VCH: Germany (1999).

[34] Fungisai Matemadombo-diploma thesis, “Substituted phthalocyanines: development and self-assempled monolayer sensor studies”, Rhosed University, January 2006.

[35]http://wwwbiol.paisley.ac.uk/marco/Enzyme_Electrode/Chapter1/Cyclic_Voltammetry1.htm

[36] Mario Birkholz, ”Thin film analysis by X-ray scattering”, WILEY-VCH Verlag GmbH & Co. KGaA Weinheim (2006).

[37] Joachim Stöhr, “NEXAFS spectroscopy”, Springer- Verlag Berlin- Heidelberg (1992).

[38] B. Johnev, K. Fostiropoulos, Solar Energy Materials & Solar Cells 92, (2008) 393–396.

[39] T. Ikame, K. Kanai, Y. Ouchi, E. Ito, A. Fujimori, K. Seki, Chemical Physics Letters 413, (2005) 373-78.

[40] Markus Plaschke, Jörg Rothe, Melissa A. Denecke, Thomas Fanghänel, Journal of Electron Spectroscopy and Related Phenomena 135, (2004) 53–62.

[41] K. K. Okudaira, H. Setoyama, H, Yagi, K. Mase, S. Kera, A. Kahn, N. Ueno, Journal of Electron Spectroscopy and Related Phenomena, (2004) 137-140.

[42] Jie Chen, L. Aé, Ch. Aichele, and M. Ch. Lux-Steiner, Applied Physics 92, (2008).

[43] B. Johnev, M. Vogel, K. Fostiropoulos, B. Mertesacker, M. Rusu, M. -C. Lux-Steiner, A. Weidinger, Thin Solid Films 488, (2005) 270 – 273.

[44] Pinyi Yang, Xiaoyuan Zhou, Gongzhong Cao and Christine K. Luscombe, J. Mater. Chem. 20, (2010), 2612-2616.

[45] Smarsly, B.; Antonietti, M. Europ. J. Inorg. Chem. 6, (2006), 1111-1119.

[46] A. A. Ebert and H. B. Gottlieb, J. Am. Chem. Soc. 74, (1952), 2806.

[47] M. D. Pirriera, J. Puigdollers, C. Voz, M. Stella, J. Bertomeu, and R. Alcubilla, J. Phys. D: Appl. Phys. 42, (2009), 145102.

[48] T. Kambayashi, H. Ohta, H. Hoshi, M. Hirano, H. Hosono, H. Takezoe, and K. Ishikawa, Cryst. Growth Des. 5, (2005), 143.

[49] Yutaka Harima, Kazuo Yamashita, Hisao Ishii, Kazuhiko Seki, Thin Solid Films 366, (2000), 237-248.

[50] P. Peumans and S. R. Forrest, Appl. Phys. Lett. 79, (2001), 126.

[51] MY Chan, SL Lai, MK Fung, CS Lee, ST Lee, Appl Phys Lett. (2007), 3.

[52] A. Yakimov, SR. Forrest, Appl. Phys. Lett. (2002), 1667–1669.

[53] T. Tsuzuki, Y. Shirota, J. Rostalski, D. Meissner, Sol. Energy Mater. Sol Cells. (2000), 8.

[54] J. Drechsel, B. Männig, F. Kozlowski, M. Pfeiffer, K. Leo, H. Hoppe, Appl Phys Lett. (2005), 3.

[55] I. Kim, HM. Haverinen, J. Li, and GE. Jabbour, Applied Physics Letters, 97, (2010).

[56] http://www.heliatek.com/?p=1923&lang=en

[57] http://lamoana.hubpages.com/hub/New-Ultrathin-Solar-Cells

Acknowledgements

For this dissertation I would like to express my gratitude to the following people:

Dr. Konstantinos Fostiropoulos, for accepting me in his scientific group. Thank you for thesis corrections. Thanks for the scientific advices. Thanks for providing everything else for our research.

Prof. Dr. Arne Thomas, for accepting me as Ph.D. student in TU-Berlin. Thank you for the scientific discussions and thesis corrections.

Prof. Bernd Smarsly, for providing me with mesoporous ITO substrates.

Wolfram Schindler, for the SEM measurements. Thanks for helping me with so many sample transfers. Thanks for being a good colleague.

Tayfun Mete, for the XRD measurements. Thank you for the funny discussions.

Fatemeh Ghany, for the AFM measurements. Thanks for the collaboration.

Sven Wiesner, for fixing of all problems with our vacuum chamber.

Dr. Boyan Johnev, for bringing me into the world of science. Thank you for the friendship.

My girlfriend Tanya, for giving me love, happiness and support all these years. Thank you for putting our relationship before everything else.

My family, for the total support. Thank you for always believing in me.